

Reactive atomistic simulations of Diels-Alder-type reactions: Conformational and dynamic effects in the polar cycloaddition of 2,3-dibromobutadiene radical ions with maleic anhydride

Uxía Rivero,^{†,‡} Haydar Taylan Turan,^{†,‡} Markus Meuwly,^{*,†} and Stefan
Willitsch^{*,†}

[†]*Department of Chemistry, University of Basel, Klingelbergstrasse 80, Basel, Switzerland*

[‡]*Contributed equally to this work*

E-mail: m.meuwly@unibas.ch; stefan.willitsch@unibas.ch

Abstract

The kinetics, dynamics and conformational specificities for the ionic Diels-Alder reaction (polar cycloaddition) of maleic anhydride with 2,3-dibromobutadiene radical ions have been studied theoretically using multisurface adiabatic reactive molecular dynamics. A competition of concerted and stepwise reaction pathways was found and both the *s-cis* and *s-trans* conformers of the diene are reactive. The analysis of the minimum dynamic path of the reaction indicates that both, rotations and vibrations of the reactant molecules are important for driving the system towards the transition state. The rates were computed as $k = 5.1 \times 10^{-14} \text{ s}^{-1}$ for the *s-cis* and $k = 3.8 \times 10^{-14} \text{ s}^{-1}$ for the *s-trans* conformer of 2,3-dibromobutadiene at an internal temperature of

300 K. The present results are to be contrasted with the neutral variant of the title system in which only the *gauche* conformer of the diene was found to undergo a considerably slower, concerted and mostly synchronous reaction driven by the excitation of rotations. The results presented here inform detailed experimental studies of the dynamics of polar cycloadditions under single-collision conditions in the gas phase.

1 Introduction

The Diels-Alder (DA) reaction in which a diene reacts with a dienophile to form a cyclic product is a widely used tool in synthetic chemistry.^{1,2} In this reaction, two σ bonds and one π bond are formed from three π bonds with a high degree of regio- and stereoselectivity. Over the past decades, a large number of experimental and theoretical studies have been devoted to studying the mechanism of DA reactions and its dependence on the geometric and electronic properties of the reactants, see, e.g., Refs.³⁻¹⁴ and references therein.

Since two bonds are formed in this reaction, questions pertaining to its concertedness and synchronicity are central to the understanding of the reaction mechanism. A reaction is considered to be concerted if the reaction pathway exhibits only a single transition state (TS) between reactants and products so that it occurs in a single step. By contrast, a stepwise mechanism involves several transition states which have to be traversed between the reactants and the products. The time elapsed between formation of the first and the second bond defines the synchronicity of the process.¹⁵ A synchronous process is necessarily concerted, but an asynchronous one can be concerted or stepwise depending on the presence or absence of intermediates. As an important implication, only the *s-cis*-conformer of the diene can react in a synchronous DA reaction, whereas both the *s-cis* and *s-trans* conformational isomers can in principle be reactive in a stepwise mechanism.

In the literature, there has been a long-standing discussion about the synchronicity and

concertedness of DA reactions.^{3,6} The textbook picture of this reaction is that of a concerted, synchronous process governed by the Woodward-Hoffmann rules involving an aromatic TS.^{2,16} However, experiments and calculations have revealed many cases which deviate from this paradigm. This is particularly the case for ionic DA reactions (polar cycloadditions) in which one of the reagents is oxidized to form a radical cation. Radical ionic variants of the DA reaction are often faster than their neutral counterparts but still show a high degree of stereoselectivity.¹⁷⁻¹⁹ A number of studies focused on the question of the conservation of orbital symmetry in these ionic reactions in view of the Woodward-Hoffmann rules which are widely used for rationalizing mechanistic aspects of neutral DA processes.¹⁹⁻²¹ In Ref.,¹⁴ it was discussed that arguments based on orbital symmetry can be misleading for polar cycloadditions. In electronic-symmetry-conserving reactions, orbital concepts should be replaced with an analysis of the symmetries of the electronic states of the various species along the entire reaction path.

Experimentally, gas-phase collision studies carried out under single-collision conditions represent a powerful tool to explore dynamic effects in elementary chemical reactions. In combination with advanced product-detection techniques such as velocity-mapped ion imaging (VMI) introduced by Eppink and Parker,²² they enable the characterization of reaction mechanisms and dynamics in unprecedented detail. In the specific context of DA reactions, previous gas-phase experiments on the polar cycloaddition between butadiene ions and ethene have been unable to isolate the DA product. As no efficient deactivation of the cycloadduct was possible in the gas phase, it was concluded that the product must have fragmented under the experimental conditions.²³ This conclusion was supported by subsequent computational studies which explored the possible fragmentation pathways of the DA product in order to interpret the experimental findings.^{24,25}

Here, the gas-phase ionic DA reaction between 2,3-dibromobutadiene radical ions (DBB⁺)

and maleic anhydride (MA) was studied by means of reactive molecular dynamics simulations. Previous work^{26,27} had revealed that the neutral counterpart of this reaction is synchronous, direct and promoted by rotational excitation of the reactant molecules. By contrast, the present work shows that the ionic system is characterized by a competition of concerted and stepwise reaction pathways and that both, the *s-cis* and *s-trans* conformers of DBB⁺ are reactive. With computed rates of $k = 5.1 \times 10^{-14} \text{ s}^{-1}$ for the *s-cis* and $k = 3.8 \times 10^{-14} \text{ s}^{-1}$ for the *s-trans* conformers of DBB⁺, respectively, at an internal temperature of 300 K and a collision energy of 100 kcal/mol, the ionic reaction was found to be considerably faster than its neutral variant under these conditions. Rotations still play a role in activating the ionic reaction, but less pronouncedly than in the neutral system. The present study highlights salient dynamic differences between neutral and ionic DA reactions and paves the way for a detailed investigation of these effects in conformationally controlled gas-phase experiments.²⁸

2 Methods

2.1 Molecular Dynamics Simulations

Atomistic simulations were carried out with the CHARMM program²⁹ using multisurface adiabatic reactive molecular dynamics (MS-ARMD).³⁰ Initial conditions for the collision simulations were generated from ensembles of the individual molecules (MA and DBB⁺) at different vibrational temperatures. Heating and equilibration temperatures were selected according to the desired final vibrational temperature (T_{vib}). The centers of mass of the two reactants were initially separated by 20 Å with a random relative orientation of the molecules. The collision energy (E_{coll}) was chosen by scaling the atomic velocities along the collision axis. Rotational energy corresponding to a particular rotational temperature (T_{rot}) was added to the molecules following calculation of their moment-of-inertia tensor and

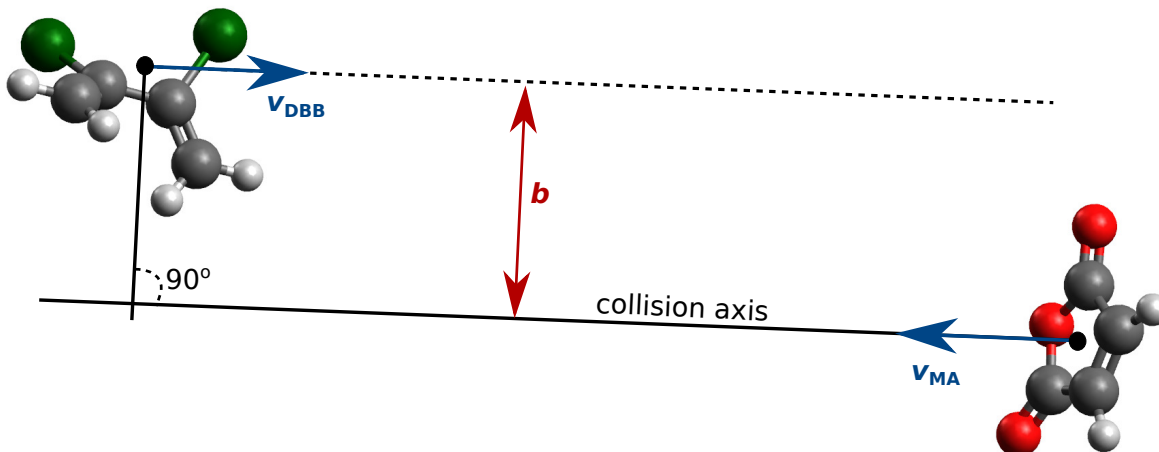


Figure 1: Schematic of the initial conditions of a trajectory. The centers of mass of the reactant molecules were initially separated by 20 Å along the collision axis. The impact parameter (b) was specified by displacing the 2,3-dibromobutadiene ion (DBB^+) along an axis perpendicular to the collision axis. The blue arrows represent the initial velocities of the centers of mass of DBB^+ (v_{DBB}) and maleic anhydride (MA, v_{MA}).

assuming equipartition among the three rotational degrees of freedom.³¹ The impact parameter (b) was uniformly sampled by displacing the center of mass of one of the molecules along an axis perpendicular to the collision axis (Figure 1). Excitation of specific vibrational modes was achieved by projecting the initial velocities onto the space of normal modes and by modifying the kinetic energy of the desired normal mode. All bonds, including those involving hydrogen atoms, were kept flexible and the time step in the simulations was sufficiently small ($\Delta t = 0.1$ fs) to ensure conservation of total energy. For propagating the equations of motion, the velocity Verlet algorithm was used.³²

2.2 Force Field Parametrization

For the reactive simulations MS-ARMD³⁰ was used. Reference calculations for the parametrization were carried out at the density functional theory (DFT) level with the M06-2X functional³³ and the 6-31G* basis set³⁴ using Gaussian09 for the electronic structure calculations.³⁵ This level of theory was previously found to yield an adequate description of the

energetics of the system of interest.²⁶ For the initial force field of reactant and product states, the parameters from SwissParam³⁶ were used. Based on those, ensembles of reactant- and product-state structures were generated with CHARMM as follows: an optimization of the structures with the Newton-Raphson method was followed by 50 ps of heating dynamics, 50 ps of equilibration at 500 K, 60 ps of cooling down to 300 K and free *NVE* (microcanonical ensemble) dynamics. The temperature was only raised up to 400 K for the reactant van-der-Waals complex to avoid dissociation. For parametrising the intermediate, the final temperature was set to 100 K to ensure obtaining low-energy structures. Additional structures for this force field were generated through scans around the first new bond formed along the reaction.

Single point energies at the M06-2X/6-31G* level of theory were computed for parametrizing the different force fields including the product state (2086 structures), the intermediate (INT-tr⁺, 1785 structures), the non-bonded interactions of the reactant (2589 structures), and the IRCs for the *endo* (169 structures), the *exo* (192 structures) and the *trans* (234 structures) paths, respectively; see Section 3.1 below for a discussion of these different structures. The harmonic bond, Morse bond, angle and dihedral parameters of MS-ARMD force fields are summarized in Tables S2 to S5 of the supplemental material (SM), respectively. Further, non-bonded parameters of reactant, intermediate and product PES are presented in Tables S6 to S8 of the SM, respectively.

In the crossing region the force fields were connected by combining the force fields of the reactants, intermediate and products with “GAussian times POLynomial” (GAPO) functions,³⁰ see supporting information. A genetic algorithm was used for fitting these GAPOs.³⁷ The global reactive potential energy surface (PES) was thus

$$V_{\text{MS-ARMD}} = \sum_{i=1}^n w_i(\mathbf{x}) V_i(\mathbf{x}) + \sum_{i=1}^{n-1} \sum_{j=1+1}^n [w_i(\mathbf{x}) + w_j(\mathbf{x})] \sum_{k=1}^{n_{ij}} \Delta V_{\text{GAPO},k}^{ij}(\mathbf{x}), \quad (1)$$

where $V_i(\mathbf{x})$ is the energy of the force field of state i (reactant, product, intermediate) at nuclear geometry \mathbf{x} , their weights $w_i(\mathbf{x})$, and the $\Delta V_{\text{GAPO},k}^{ij}(\mathbf{x})$ are GAPO functions up to third (for reactant and intermediate) and second (for intermediate and product) polynomial order, respectively, see Table S9 of the SM. In order to render the force field permutation invariant, two and four different force fields for the description of the product and the intermediate were used, respectively (see Tables S2 to S8 of the SM).

2.3 Analysis of the Trajectories

Reactive trajectories were analyzed by decomposing the energy content of the fragments along different degrees of freedom. For this purpose, the total kinetic energy along the minimum dynamic path³⁸ (Section 3.2) was analyzed in two ways. In one approach, the total kinetic energy was projected onto the eigenvectors of the Hessian matrix of the reactant molecules with geometries corresponding to the last point of each trajectory. Alternatively, the total kinetic energy was decomposed into the translational energy of the center of mass of the reactant molecules (E_{trans}), and their rotational (E_{rot}) and vibrational (E_{vib}) energy. The translational energies were calculated according to

$$E_{\text{trans},A} = \frac{\left| \sum_{i \in A} \vec{p}_i \right|^2}{2M_A}, \quad (2)$$

where \vec{p}_i is the momentum of atom i belonging to molecule A ($A = \text{MA}, \text{DBB}^+$) and M_A is the total mass of molecule A. The rotational energies were computed as

$$E_{\text{rot},A} = \frac{1}{2} |\mathbf{I}_A \vec{\omega}_A^2|. \quad (3)$$

Here, $\vec{\omega}_A$ is the angular velocity of molecule A and \mathbf{I}_A is the moment-of-inertia tensor of molecule A,

$$\vec{\omega}_A = \mathbf{I}_A^{-1} \vec{L}_A. \quad (4)$$

In this equation, \vec{L}_A is the angular momentum of molecule A,

$$\vec{L}_A = \sum_{i \in A} \vec{r}_i' \times \vec{p}_i', \quad (5)$$

where atomic momenta (\vec{p}_i') and atomic coordinates (\vec{r}_i') in the center of mass frame were calculated as:

$$\vec{x}_i' = \vec{x}_i - \vec{x}_{\text{CoM},A}; \quad x = p, r \quad (6)$$

and the subscript "CoM, A" refers to the center of mass of molecule A. Finally,

$$E_{\text{vib},A} = E_{\text{tot},A} - E_{\text{rot},A} - E_{\text{trans},A} \quad (7)$$

where $E_{\text{tot},A}$ is the total kinetic energy of molecule A along the trajectory.

The trajectories were considered reactive and terminated when they reached the product force field. The reactive cross section σ was calculated according to

$$\sigma = 2\pi b_{\text{max}} \frac{1}{N_{\text{tot}}} \sum_{i=1}^{N_{\text{reac}}} b_i, \quad (8)$$

where b_{max} is the maximum impact parameter (defined as the impact parameter at which no reactions could be observed anymore), N_{tot} is the total number of trajectories, N_{reac} is the number of reactive trajectories and b_i is the impact parameter of the reactive trajectory i .

3 Results and Discussion

3.1 Parametrization of the Reactive Force Fields

Figure 2 shows stationary points on the PES of the Diels-Alder reaction between DBB⁺ and MA at the M06-2X/6-31G* level of theory.²⁶ For the *s-cis* conformer of DBB⁺ both reactant molecules (DBB⁺ and MA) are symmetric. Thus, there are two possible pathways for a concerted Diels-Alder reaction referred to as “*endo*” and “*exo*” depending on the relative orientation of the reactants (Figures 2 (a) and (b)). For the *exo* configuration, an additional stepwise pathway via an intermediate INT-*exo*⁺ was identified (Figure 2 (b)). For the *s-trans* conformer of DBB⁺, a stepwise pathway was found (“*trans*”, Figure 2 (c)). The *endo* product (P-*endo*⁺) was defined as the zero of the energy scale in Figure 2.

The aim of the present parametrization was to obtain a single, globally valid reactive MS-ARMD PES that describes the three competing paths, see Figure 2, as had previously been done for competitive ligand binding.³⁹ The *endo* intrinsic reaction coordinate (IRC, Figure 2 (a)) was used for parametrizing the GAPOs. It is important to mention that the *endo* IRC is asymmetric since it exhibits a plateau after the transition state (see Figure S1 of the SM). The structures in this region resemble those of the intermediate state with one of the new C-C bonds formed. Hence, the intermediate force field is active in this region which is an approximation because the *endo* path has no minimum there. However, this was the only viable way to obtain a single global PES.

The quality of the reactive PES compared with the reference DFT data is reported in Figure 3. The total root-mean-square deviation (RMSD) is 2.9 kcal/mol over a range of 120 kcal/mol which is deemed sufficient for a correct qualitative characterization of the dynamics of the system. There are some outliers in the intermediate force field (INT⁺ in Figure 3). However, because they have high energies in the parametrized PES, the system will rarely sample

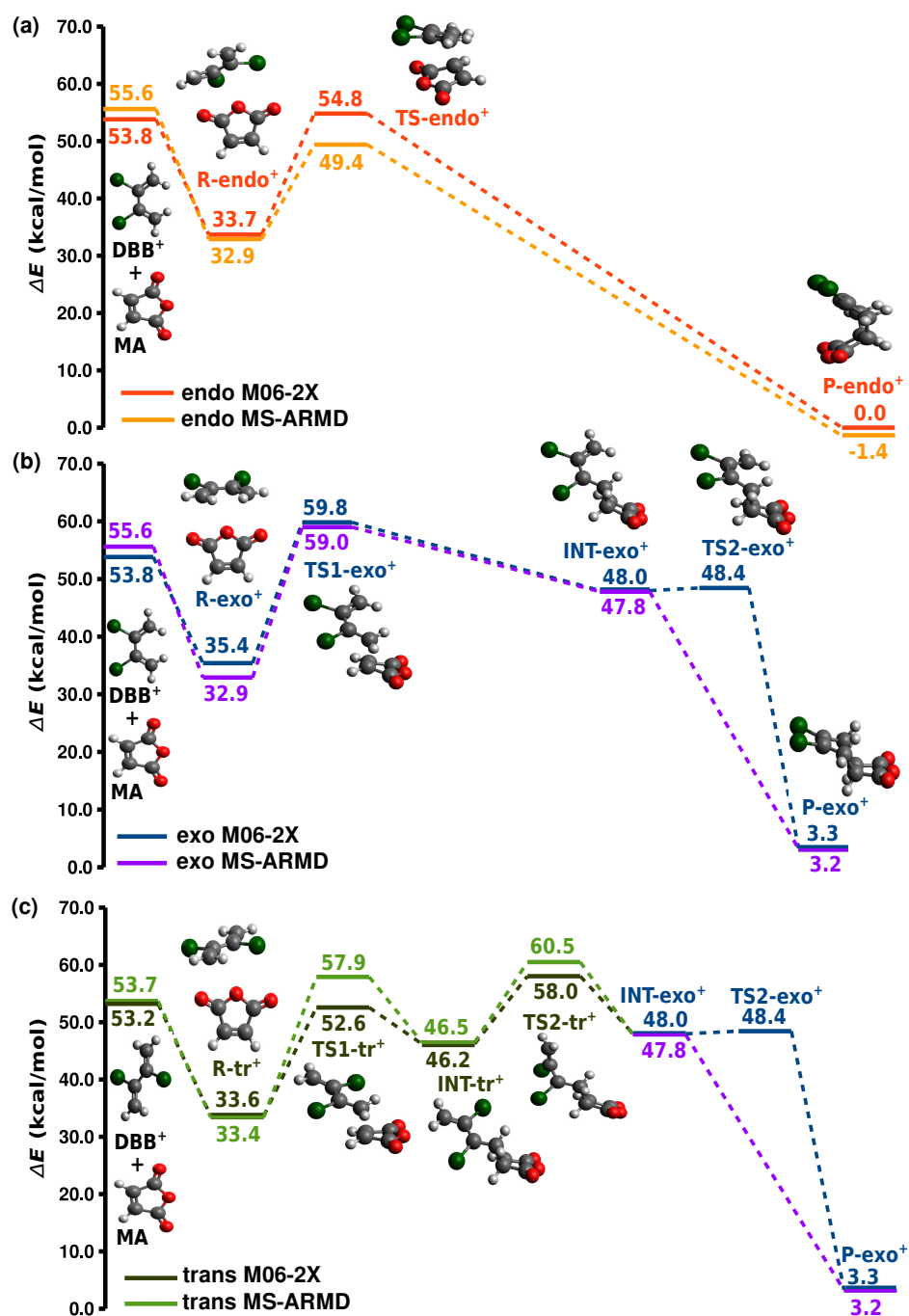


Figure 2: Potential energy surface for the three possible DA reaction paths (a) *endo*, (b) *exo* and (c) *trans* between 2,3-dibromobutadiene cation (DBB⁺) and maleic anhydride (MA) at the M06-2X/6-31G* level of theory and from MS-ARMD. Relative energies are given in kcal/mol with respect to the *endo* product (P-endo). The structures are connected by minimum-energy paths (indicated as dashed lines) verified by intrinsic-reaction-coordinate (IRC) calculations. The superscripts "+" indicate ionic structures.

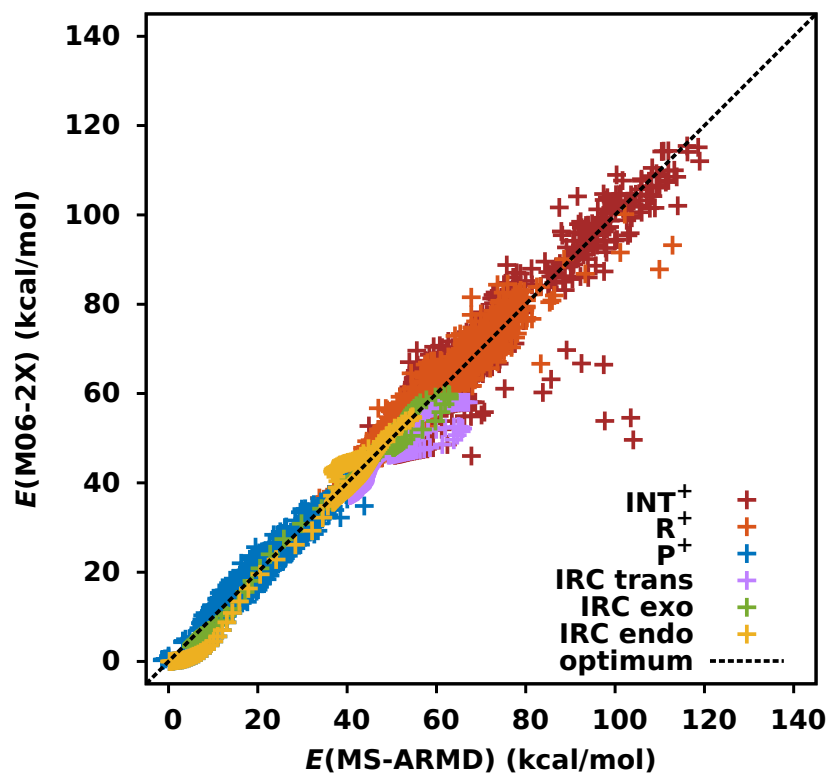


Figure 3: Energy correlation of 7055 reference structures computed at the M06-2X/6-31G* level of theory and the MS-ARMD PES. The total root-mean-square deviation (RMSD) is 2.9 kcal/mol.

these regions which are thus expected to have a minor impact on the dynamics.

Figure 2 compares the MS-ARMD energies with those from the reference DFT calculations. The *exo* path (Figure 2(b)) is well described although TS2- exo^+ does not exist on the MS-ARMD surface. As discussed above, the total RMSD of the surface is 2.9 kcal/mol and so it is expected that a TS that lies 0.4 kcal/mol above the minimum INT- exo^+ is not captured by the parametrized force field. The *endo* path (Figure 2(a)) exhibits a TS 5.4 kcal/mol lower than the reference energy which implies that the Diels-Alder reaction along this path is more favorable when treated with the MS-ARMD PES than the dissociation of the van der Waals complex in the entrance channel, while at the DFT level the heights of the barriers towards dissociation and the onward reaction are similar. This mismatch will lead to overestimating the reaction rate along the *endo* path in MS-ARMD. Finally, for the *trans* path (Figure 2(c)), the energies of TS1- tr^+ and TS2- tr^+ are overestimated by 5.3 kcal/mol and 2.5 kcal/mol, respectively. The overestimation of the energy of the first TS should not be worrisome, because the bottleneck for the reaction along this path is TS2- tr^+ which lies higher in energy than TS1- tr^+ for both, the MS-ARMD PES and the reference DFT calculations. However, the higher energy of TS1- tr^+ in the MS-ARMD treatment will artificially extend the lifetime of INT- tr^+ .

In addition to comparing energies for stable and transition states, their geometries and harmonic frequencies were determined from the MS-ARMD PES and from the reference DFT calculations, see Figures S2 and S3 and Table S1 of the SM. A superposition of the reactant, intermediate, transition-state and product structures is shown in Figure S2 of the SM and the root mean squared differences are reported in Table S1 of the SM. The monomeric structures superimpose to within better than 0.1 Å which indicates that the bonded parameters of the MS-ARMD force field are reliable. For the complex structures the product and intermediate states show deviations of up to 0.2 Å which increase to ~ 0.3 Å for transition state structures.

This suggests that further optimization of the nonbonded parameters (charges and van der Waals) may be possible. The harmonic frequencies along the *endo* path from MS-ARMD and the DFT calculations agree very favorably, see Figure S3a of the SM which underlines the quality of the reaction path for which the GAPOs were parametrized. These parameters do, however, not yield the same quality for the *exo* and *trans* paths, in particular for the intermediate and high frequencies for the INT⁺ and TS2⁺ structures (Figures S3b and c). Of course, dedicated parametrization of these two paths with increased accuracy would be possible but only at the expense of a reduced generality of the global energy function.

It is important to remember that the intermediate region of the PES is quite flat reflecting that the intermediate structure is much more flexible and samples a wider range of conformations compared to the reactants or the products. Therefore, the reference data points on this part of the surface are expected to be of lower quality than those in the reactant and the product regions.²⁶ For this reason, special care is needed in the analysis of trajectories that extensively sample the intermediate-state region of the PES where the parametrization is less accurate than for the reactant and product geometries. Because the aim was to develop a single reactive force field for the *s-cis* intermediate along the *exo* path (Figure 2(b)) and the *trans* intermediate (Figure 2(c)) in order to arrive at a global treatment of all reaction pathways, the charges and equilibrium distances of bonds and angles are identical for both these intermediates.

3.2 Minimum Dynamic Path

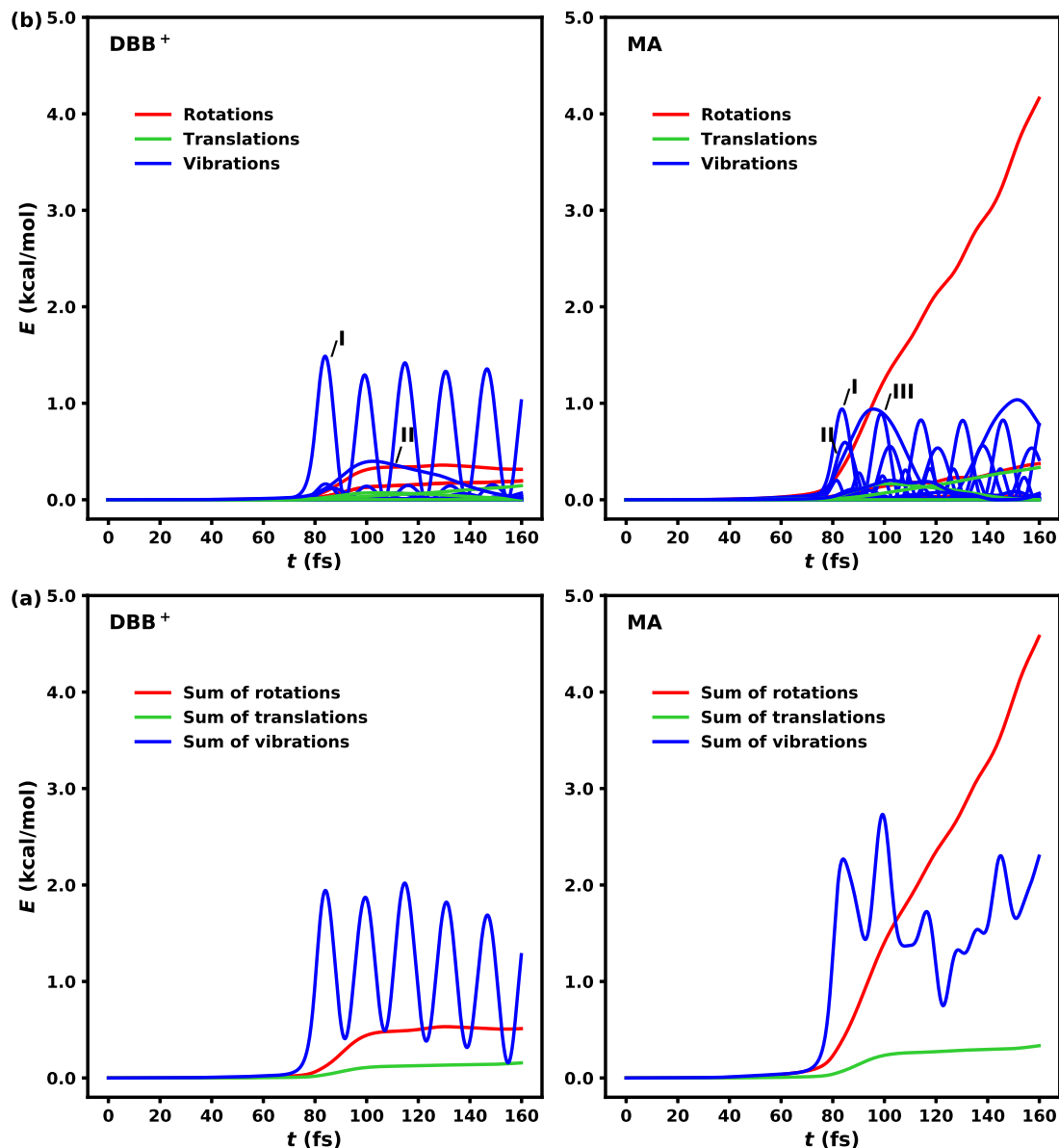


Figure 4: The MDP starting from TS1-exo⁺. Projection of the total kinetic energy (E) onto the degrees of freedom of the 2,3-dibromobutadiene ion (DBB⁺) and maleic anhydride (MA) along the minimum dynamic path for the reaction of *s-cis*-DBB⁺ + MA (a) summed into rotations, translations and vibrations and (b) further decomposed into individual components of the different degrees of freedom. The predominant active vibrations identified for DBB⁺ are: (I) out-of-plane symmetric bending of hydrogens, and (II) skeleton out-of-plane asymmetric bend (*cis/trans* isomerization mode); for MA: (I) and (II) asymmetric and symmetric out-of-plane hydrogen bending, respectively, and (III) asymmetric C=C out-of-plane bending.

The minimum dynamic path (MDP) is the lowest-energy dynamical path that follows Newton’s equations of motion in phase space.³⁸ A trajectory starting at a TS geometry without kinetic energy follows the MDP. The MDP was calculated for the three different reaction pathways in the same fashion as previously for the neutral reaction in Ref.²⁷ The following discussion will be centered around the *exo* path because it is best described by the present MS-ARMD PES (Figure 4). However, since the *endo* and *trans* paths are energetically more favorable, the MDPs of these two pathways are also shown (Figures 5 and 6).

For the *exo* pathway, the projection of the total kinetic energy along the MDP towards the reactants onto the degrees of freedom of DBB⁺ and MA is shown in Figure 4(a) as sums of the translational, rotational and vibrational energies. At $t = 0$ fs the system is at TS1-*exo*⁺ and at $t = 160$ fs it has arrived at the reactants state. By projecting the total kinetic energy onto the different degrees of freedom of DBB⁺ and MA, the active degrees of freedom in this reaction could be identified. Figure 4(a) shows that the largest amount of energy is partitioned into the vibrations of DBB⁺, while rotations contain the largest amount of energy for MA although vibrations are also active (see individual contributions in Figure 4(b)). The rotational energy of DBB⁺ and MA together accounts for 46% of the total kinetic energy while vibrational energy accounts for 48% and translational energy for only 6%. The same result was obtained from the direct decomposition of the total kinetic energy (see Figure S4 of the SM). This finding stands in clear contrast to the neutral DBB + MA system explored in Ref.²⁷ for which rotations accounted for 63% of the total kinetic energy and vibrations and translations for only 19% and 18%, respectively.

The pronounced excitation of vibrational modes can be traced back to the asymmetry of the cationic TS the breakup of which deforms the molecules more strongly than in the neutral variant of the reaction which exhibits a symmetric TS. On the grounds of microscopic reversibility, the excitation of these vibrations is expected to promote the reaction on its way

towards the TS which provides valuable information about future, possible experiments on this system.

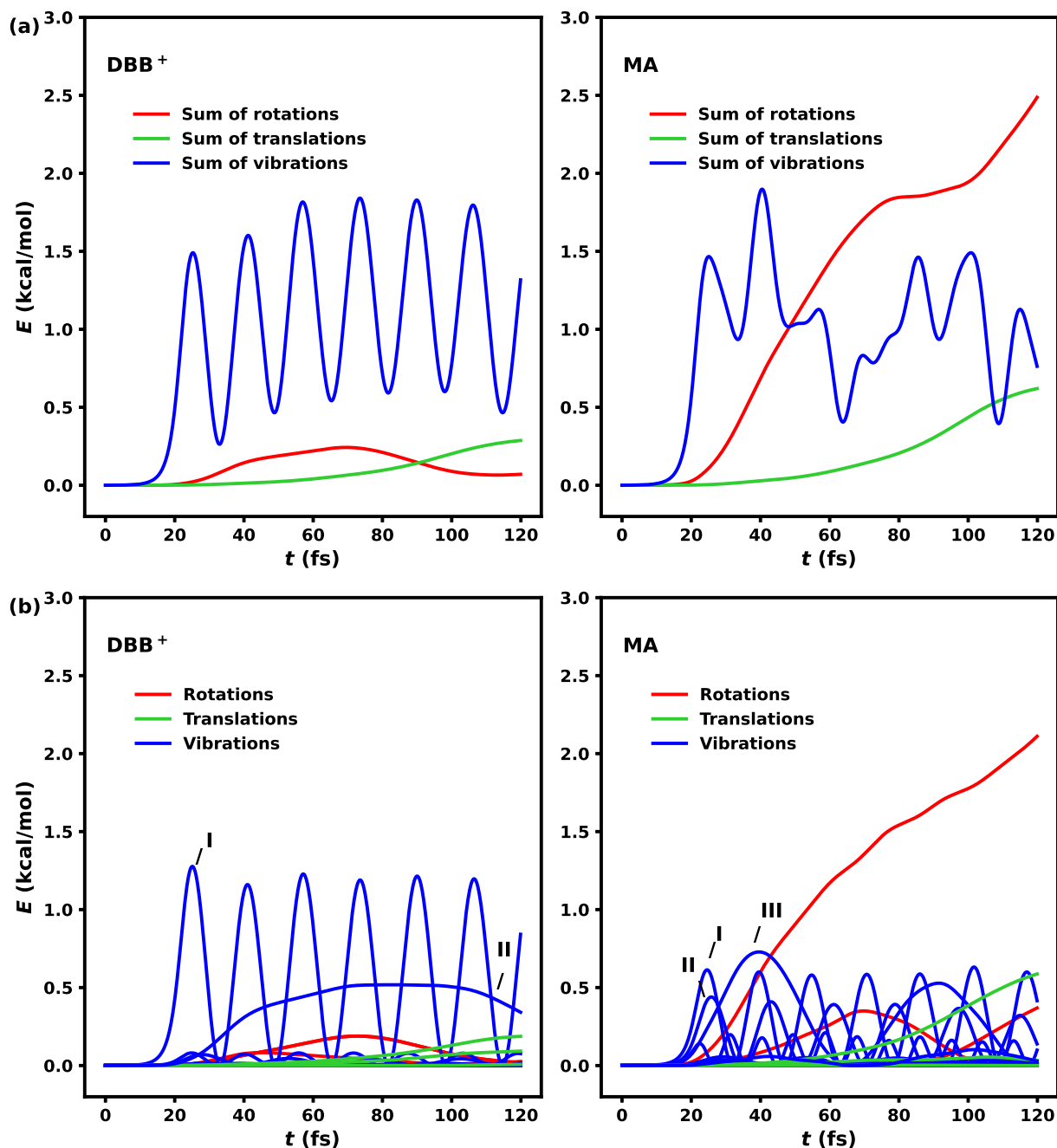


Figure 5: The MDP starting from TS-endo⁺. Projection of the total kinetic energy (E) onto the degrees of freedom of the 2,3-dibromobutadiene ion (DBB⁺) and maleic anhydride (MA) along the minimum dynamic path for the reaction of *s-cis*-DBB⁺ + MA (a) summed into rotations, translations and vibrations (b) as individual traces. The predominant active vibrations identified for DBB⁺ are: (I) out-of-plane symmetric bending of hydrogens and (II) skeleton out-of-plane asymmetric bend (*cis/trans* isomerization mode); for MA: (I) and (II) asymmetric and symmetric out-of-plane hydrogen bending, respectively and (III) asymmetric C=C out-of-plane bending.

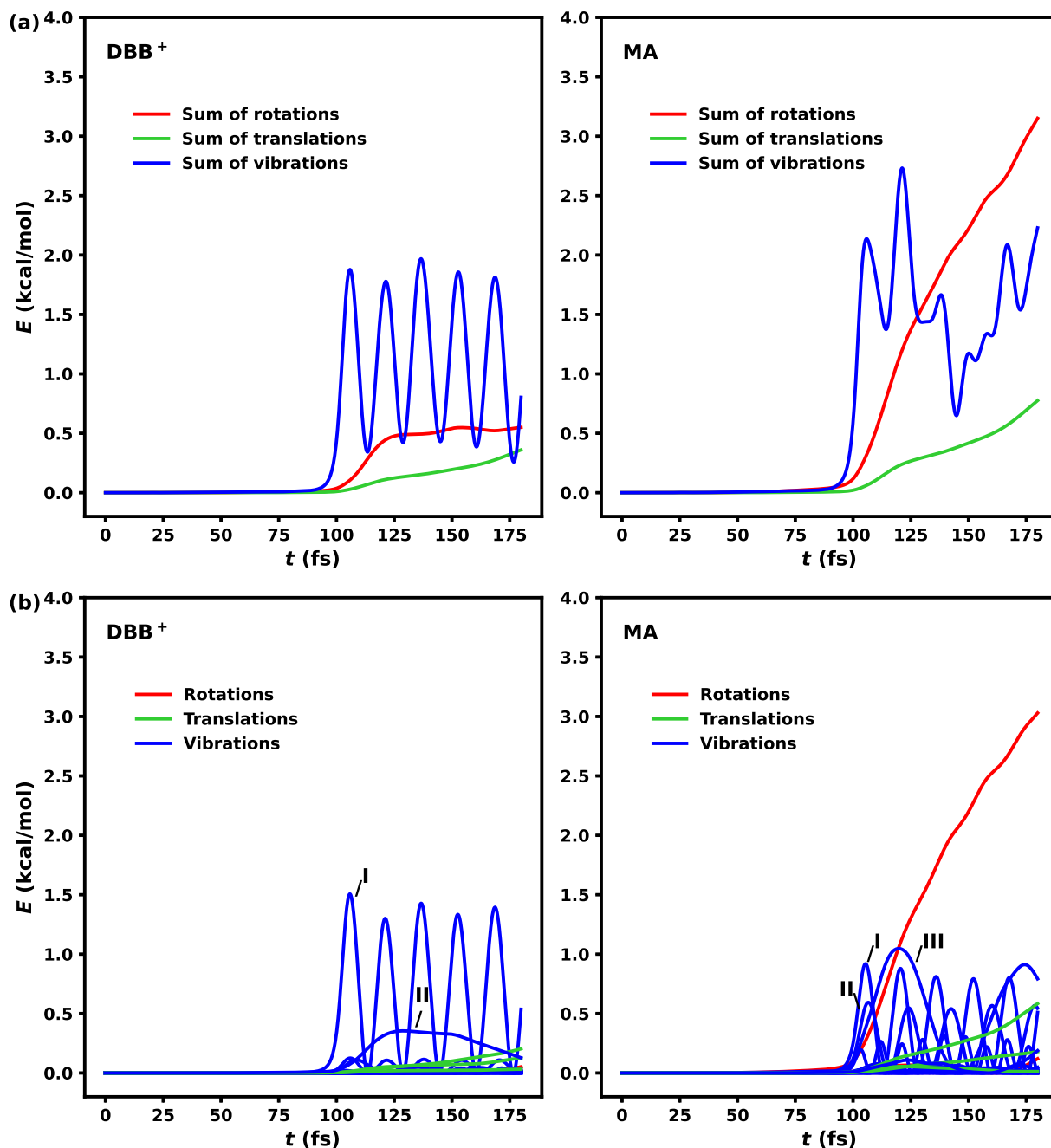


Figure 6: The MDP starting from TS1-trans⁺. Projection of the total kinetic energy (E) onto the degrees of freedom of the 2,3-dibromobutadiene ion (DBB⁺) and maleic anhydride (MA) along the minimum dynamic path for the reaction of *s-trans*-DBB⁺ + MA (a) summed into rotations, translations and vibrations (b) as individual traces. The predominant active vibrations identified for DBB⁺ are: (I) out-of-plane symmetric bending of hydrogens and (II) skeleton out-of-plane symmetric bend; for MA: (I) and (II) asymmetric and symmetric out-of-plane hydrogen bending, respectively and (III) asymmetric C=C out-of-plane bending.

The projection of the total kinetic energy onto the degrees of freedom of DBB⁺ and MA along the *endo* and *trans* MDPs are reported in Figures 5 and 6, respectively. For the *endo* path, vibrational energy accounts for 54% of the total kinetic energy while rotational and translational degrees of freedom contain 38% and 8%, respectively. This suggests that rotational energy is less important to drive the reaction along the *endo* path compared to the *exo* path, see Figure 4. For the *trans* pathway, the contributions of vibrational, rotational and translational energy are 50%, 40% and 10%, respectively. The active vibrations of MA were found to be the same in all paths. For DBB⁺, they remain the same for the *endo* and *exo* trajectories and one mode changes for the *trans* path because the conformation of the molecule is different.

The MDP for the *cis/trans* isomerization of INT⁺ has also been calculated. The total kinetic energy along this trajectory has been projected onto the degrees of freedom of INT-tr⁺ as shown in Figure S5 of the SM. The energy is essentially exclusively partitioned into vibrations as is expected for a unimolecular reaction. The most active vibration is the *cis/trans* isomerization mode. Other low frequency skeleton vibrations are also slightly active.

3.3 Cross sections for the formation of van-der-Waals complexes in the entrance channel

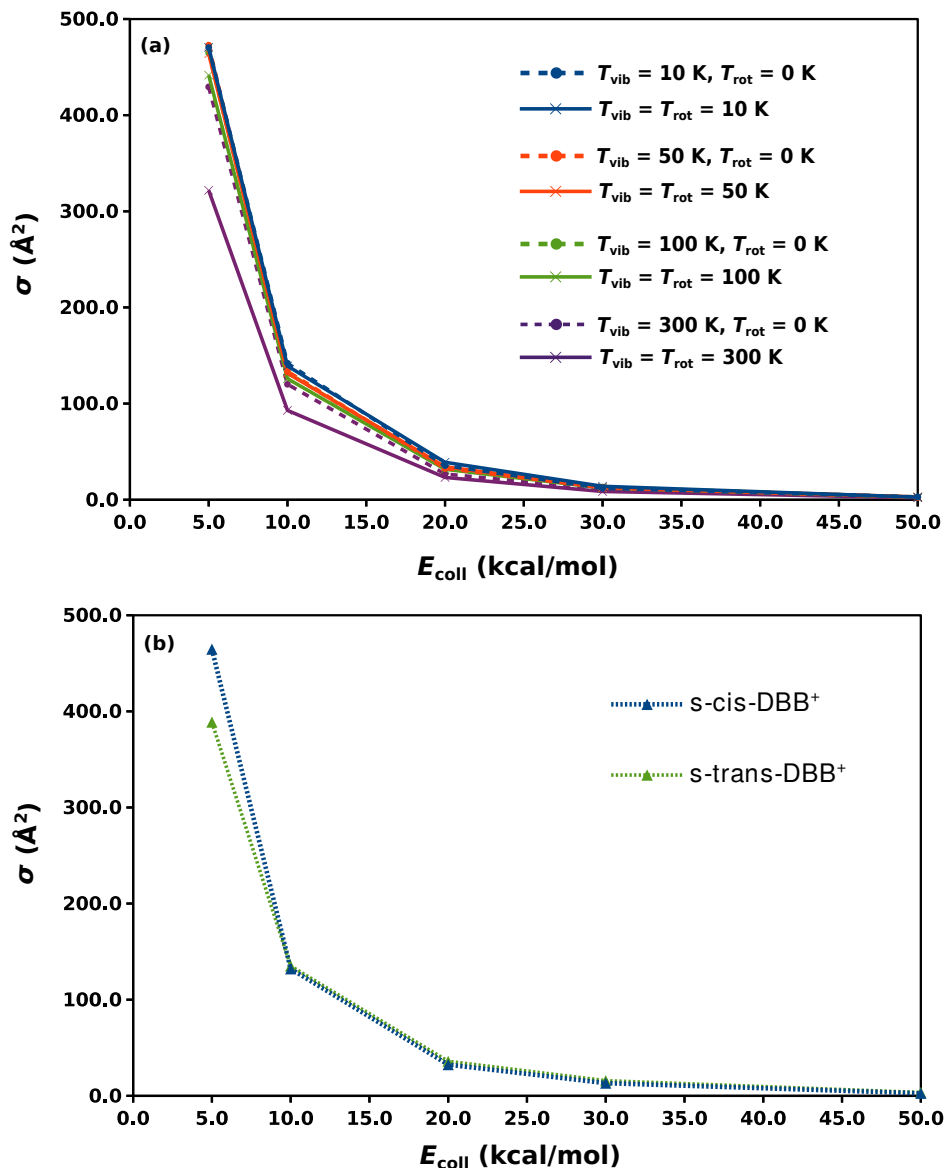


Figure 7: (a) Variation of the cross section (σ) for the formation of the van-der-Waals complex in the entrance channel of the Diels-Alder reaction between *s-cis*-2,3-dibromobutadiene ions (DBB^+) and maleic anhydride (MA) as a function of the collision energy (E_{coll}) at different vibrational and rotational temperatures (T_{vib} , T_{rot}). (b) Comparison of the cross sections for the *s-cis* and *s-trans* conformers of DBB^+ at $T_{\text{vib}} = 100 \text{ K}$ and $T_{\text{rot}} = 0 \text{ K}$.

The formation of van-der-Waals complexes in the entrance channel was studied in order to establish whether the reaction is direct (i.e., without the formation of complexes) or

complex-mediated. The impact parameter b was uniformly sampled in intervals of 1 Å up to a maximum value b_{max} at which no reactive collisions could be observed anymore. For each set of initial conditions $(E_{\text{coll}}, T_{\text{vib}}, T_{\text{rot}}, b)$, 500 trajectories were run for 10 ps. If at the end of a trajectory the center-of-mass distance between the two molecules was < 15 Å, it was concluded that a van-der-Waals complex had been formed. Figure 7(a) shows the cross section σ for the formation of complexes as a function of the collision energy. It can be seen that σ diminishes as the collision energy increases. Comparing to the neutral variant of the reaction studied in Ref.,²⁷ the maximum cross section computed is $\sigma_{\text{max}} \approx 475 \text{ Å}^2$, while for the neutral case $\sigma \approx 110 \text{ Å}^2$ was found. In addition, the cross section for the ionic reaction decreases much slower with collision energy and only totally vanishes at $E_{\text{coll}} > 50 \text{ kcal/mol}$. Rotational and vibrational energy have less influence than in the neutral case. All these results reflect the fact that the van-der-Waals complex in the entrance channel of the ionic reaction is $\approx 12 \text{ kcal/mol}$ more stable than the one in the neutral variant.

The influence of the initial conformation of DBB^+ in the cross section for the formation of a van der Waals complex in the entrance channel is shown in Figure 7(b). It can be seen that there is only a small difference at the lowest collision energies at which the cross section for the *s-cis* species is higher than for the *s-trans* conformer due to the fact that the maximum impact parameter for complex formation was found to be $b_{\text{max}} = 16 \text{ Å}$ for *s-cis*- DBB^+ while it is 14 Å for *s-trans*- DBB^+ . However, these differences are judged to be too small to be really significant.

3.4 Reaction cross sections and rates

The dynamics of the full reaction was investigated in two steps. First, head-on collisions (i.e., $b = 0$) were considered in order to obtain an overview of the number of trajectories required and the reaction rates to be expected. This was followed by a more comprehen-

sive study of off-axis collisions with $b > 0$. Such a procedure is warranted based on the previous finding for the neutral reaction in which $\sim 10^7$ trajectories only lead to ~ 500 reactive events.²⁷ Also, head-on collisions were found to be most effective for the neutral reaction.

Table 1: Initial conditions sampled for the recorded reactive events in terms of collision energy (E_{coll}), conformation of the 2,3-dibromobutadiene ion (DBB⁺) and rotational temperature (T_{rot}) at a vibrational temperature $T_{\text{vib}} = 100$ K and impact parameter $b = 0$ Å. All simulations were propagated until dissociation or until they reached the products up to a total time of $t = 600$ ps except for those with initial conditions $E_{\text{coll}} = 50$ kcal/mol, $T_{\text{rot}} = 0$ K that were only propagated until $t = 300$ ps.

E_{coll} (kcal/mol)	DBB ⁺	T_{rot} (K)	# Products	# Intermediates	# Complexes
50*	<i>s-cis</i>	0	1	19	13644
50*	<i>s-trans</i>	0	0	7	14828
50	<i>s-cis</i>	2000	24	14	829
50	<i>s-trans</i>	2000	7	25	884
50	<i>s-cis</i>	4000	57	34	33
50	<i>s-trans</i>	4000	29	40	50
75	<i>s-cis</i>	0	18	13	104
75	<i>s-trans</i>	0	4	3	174
75	<i>s-cis</i>	2000	43	20	5
75	<i>s-trans</i>	2000	22	15	17
75	<i>s-cis</i>	4000	106	19	5
75	<i>s-trans</i>	4000	69	29	23
100	<i>s-cis</i>	0	30	4	0
100	<i>s-trans</i>	0	6	0	0
100	<i>s-cis</i>	2000	92	0	0
100	<i>s-trans</i>	2000	47	3	2
100	<i>s-cis</i>	4000	153	0	0
100	<i>s-trans</i>	4000	65	0	0
Total	$1.8 \cdot 10^6$ trajectories		773	245	30598

For studying the full reaction, $1.8 \cdot 10^6$ MD simulations were carried out. The vibrational temperature was set to $T_{\text{vib}} = 100$ K to mimic vibrationally cold molecules in collision experiments involving supersonic molecular beams and trapped ions.^{40,41} Collision energies of

$E_{\text{coll}} = 50, 75$ and 100 kcal/mol were sampled. The rotational temperatures considered were $T_{\text{rot}} = 0, 2000$ and 4000 K such that the influence of rotational excitation could be studied. The trajectories started with either *s-cis*-DBB⁺ or *s-trans*-DBB⁺ (see Table 1). However, trajectories starting in the *s-trans* conformer need not necessarily follow the *trans* path (Figure 2 (c)) as DBB⁺ can isomerize upon collision with MA.

The trajectories were propagated until a) dissociation of the van-der-Waals complex back to the products occurred, b) the products were formed, or c) a maximum simulation time of $t = 600$ ps was reached. Because of the long lifetime of the van-der-Waals complexes formed under initial conditions $E_{\text{coll}} = 50$ kcal/mol, $T_{\text{rot}} = 0$ K, these trajectories were only propagated out to 300 ps because reactions typically occurred within a few ps (see below).

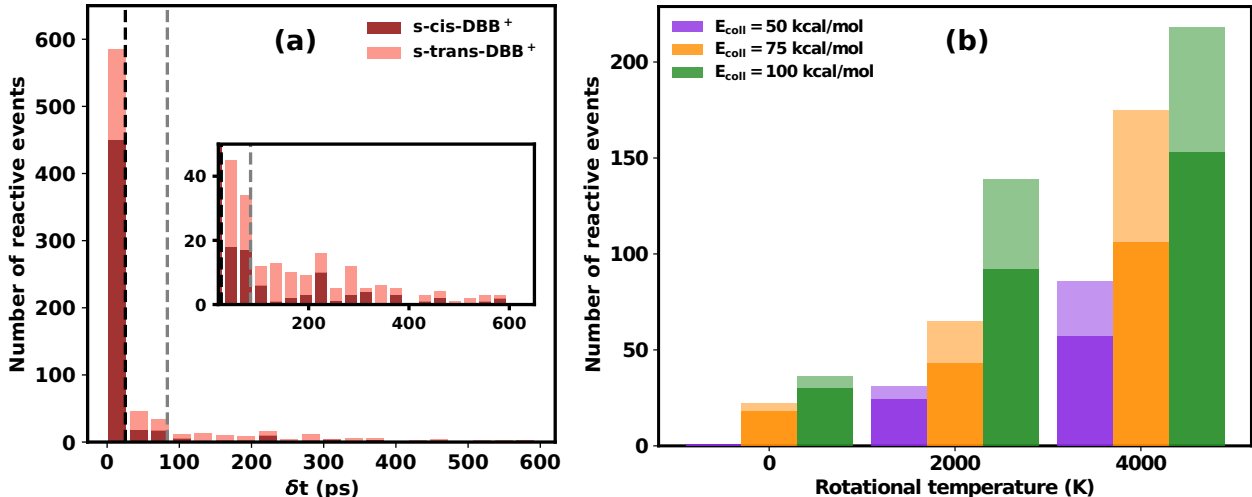


Figure 8: (a) Stacked histogram of the elapsed time (δt) for successful reactive events. Trajectories starting with *s-cis* and *s-trans*-DBB⁺ are shown in dark and light brown, respectively. The mean of the distributions are indicated as dashed black and grey vertical lines for *s-cis*-DBB⁺ and *s-trans*-DBB⁺, respectively. The inset shows a magnification of the tail of the distribution. (b) Stacked histogram of the variation of the number of reactive events at collision energies 50, 75 and 100 kcal/mol with vibrational temperature 100 K and impact parameter $b = 0$ Å as a function of the rotational temperature of the reactant molecules. Reactive events from trajectories that started with *s-cis* and *s-trans*-DBB⁺ are represented in solid and transparent colors, respectively.

As the MDP suggested and Figure 8(b) confirms, rotational energy promotes the reaction

even if the rotational degrees of freedom are less active for the ionic MDP than for the neutral reaction.²⁷ In fact, there are almost five times more reactive events at $E_{\text{coll}} = 75$ kcal/mol, $T_{\text{rot}} = 4000$ K than at $E_{\text{coll}} = 100$ kcal/mol, $T_{\text{rot}} = 0$ K even though these scenarios exhibit similar total kinetic energies.

To assess whether the reaction is direct or complex-mediated, the time t_1 of surface crossing between the reactant and intermediate force fields is shown in Figure S6 of the SM for all reactive trajectories. It was found that $t_1 < 2$ ps for the majority of trajectories and that $t_1 < 7$ ps for all reactive trajectories indicating that they are direct events. Further, the times of surface crossing for $b \in [0, 6]$ are summarized in Figures S7 and S8 of the SM for *s-cis*- and *s-trans*-DBB⁺, respectively. The majority of these reactive trajectories exhibited a reaction time between 0.5 to 1 ps. Reaction times longer than 5 ps have not been observed for either conformer.

To determine the synchronicity of the reactions, the time δt elapsed between formation of the first and second carbon-carbon bond was calculated for all reactive events as the time difference between the crossing from the reactant force field to the intermediate force field (t_1) and the crossing from the intermediate force field to the product force field (t_2) (Figure 8(a)), i.e. $\delta t = t_2 - t_1$. The times t_1 and t_2 are only approximate time stamps for the formation of the first and second bonds since the system crosses surfaces at C-C distances longer than 1.6 Å that is the usual threshold for formation of these type of bonds. However, if the system remains on the intermediate force field (for t_1) and the product force field (for t_2) the bond is formed because otherwise the system would cross back to the reactant-state PES. Out of 773 reactive events, only 59 were found to be synchronous with $\delta t < 30$ fs^{5,8} (see Table 1). All synchronous processes start from *s-cis*-DBB⁺. The intermediate species has lifetimes on the order of picoseconds. It is important to remember that our model is expected to somewhat overestimate the lifetime of the intermediate due to the high activation

barriers along the *trans* path (Figure 2(c)).

At the end of the maximum simulation time interval, there were still ~ 30000 van der Waals complexes left from the original sample of trajectories (see Table 1) that could eventually form products on longer time scales. However, no product formation with $t_1 > 7$ ps was recorded even though some of the van der Waals complexes live for 600 ps, so this is expected to be an unlikely and slow process. Nevertheless, the effect of these complexes on the total rate could be included once a direct comparison with experiment is possible.^{42,43} The 245 trajectories that are trapped in the intermediate region could eventually evolve to products or dissociate. However, as can be seen in Figure 8(a), formation of the second bond on the > 100 ps time scale after the first bond was formed only occurs in $< 1\%$ of the cases. Therefore, the contribution of such trajectories to the final rate is expected to be small.

After this qualitative overview of the reactive dynamics, the rate of reaction was estimated from a second set of trajectories by scanning the impact parameter b over a finite range. For these studies, $7 \cdot 10^5$ and $6 \cdot 10^5$ initial structures for the *s-cis*-DBB⁺ and *s-trans*-DBB⁺ conformers were generated, respectively. The impact factor (b) was chosen between 0 and 6 Å and was uniformly sampled in six non-overlapping intervals, with increments of 1 Å. For every interval, 10^5 reactive MD simulations were run. Further, 10^5 trajectories were simulated with $b = 0$ Å for both conformers to connect with the first set of simulations as described above. The collision energy was set to 100 kcal/mol, and the trajectories were simulated for 50 ps with $\Delta t = 0.1$ fs and at 300 K. The two sets of simulations were found to be consistent with one another as for $b = 0$ the fraction of reactive trajectories from the first set is 4.3×10^{-4} , compared with 4.6×10^{-4} from the second set for the same simulation conditions.

Table 2: Number of reactive trajectories at specific impact parameters b for *s-cis*-DBB⁺ and *s-trans*-DBB⁺.

$b / \text{\AA}$	0	0-1	1-2	2-3	3-4	4-5	5-6
<i>s-cis</i> -DBB ⁺	133	140	76	22	10	2	0
<i>s-trans</i> -DBB ⁺	64	72	46	33	4	0	-

The opacity functions for *s-cis*-DBB⁺ and *s-trans*-DBB⁺ (see Table 2) are presented in Figure 9. The *s-cis*-conformer was found to have a higher reaction probability for all impact factors, except around $b \sim 3 \text{\AA}$. For head-on collisions ($b = 0$), the number of reactive trajectories was 133 for *s-cis*- and 64 for *s-trans*-DBB⁺, respectively, which is consistent with the extended set of dynamics computed for $b = 0$ discussed above. For $b \in [0, 1] \text{\AA}$ the number of reactive trajectories increases slightly to 140 and 72 for *s-cis*- and *s-trans*-DBB⁺, respectively. However, this increase may not be statistically significant considering the still relatively small numbers of reactive events sampled. For larger impact parameters, the opacity function decays monotonically to reach zero around $b \in [5, 6] \text{\AA}$ for *s-cis*- and around $b \in [4, 5] \text{\AA}$ for *s-trans*-DBB⁺. Therefore, no simulations were carried out for $b \in [5, 6] \text{\AA}$ for *s-trans*-DBB⁺.

The reaction rates for the two conformers were calculated from the opacity functions. For a uniform sampling, all trajectories were grouped in non-overlapping intervals of b with a weight

$$w = \frac{2b}{b_{\max}} \quad (9)$$

where b_{\max} is the maximum value of b for which a reactive complex is formed, i.e. $b_{\max} = 5 \text{\AA}$ for *s-trans*-DBB⁺ and $b_{\max} = 6 \text{\AA}$ for *s-cis*-DBB⁺.

The reaction probability in each interval was calculated as

$$P_c = \frac{N'_r}{N_{\text{tot}}}. \quad (10)$$

Here, N_r' is the effective number of reactive trajectories,

$$N_r' = \sum_{i=1}^{N_r} w_i, \quad (11)$$

where N_r and N_{tot} is the number of reactive and total trajectories within the specific interval, respectively.

The rate coefficient was determined according to

$$k(T) = \sqrt{\frac{8k_bT}{\pi\mu}} \pi b_{\text{max}}^2 P_c. \quad (12)$$

yielding $k = 5.116 \times 10^{-14} \text{ s}^{-1}$ for *s-cis*-DBB⁺ and $k = 3.796 \times 10^{-14} \text{ s}^{-1}$ for *s-trans*-DBB⁺ at an interval, i.e., rotational-vibrational, temperature of 300 K and a collision energy of 100 kcal/mol.

Comparing with the neutral variant of the reaction, it can be concluded that the ionic system is considerably more reactive. This is exemplified by the ratio between the reactive number of trajectories and the total number trajectories which was found to be 6.79×10^{-5} in the neutral system²⁷ and 4.29×10^{-4} for the ionic reaction studied here, i.e. a difference of about one order of magnitude. For the neutral reaction comparable rates as for the ionic system were only obtained at markedly higher rotational temperatures of $T_{\text{rot}} = 4000 \text{ K}$,²⁷ while at $T_{\text{rot}} = 300 \text{ K}$, only a negligibly small number of reactive events was observed.

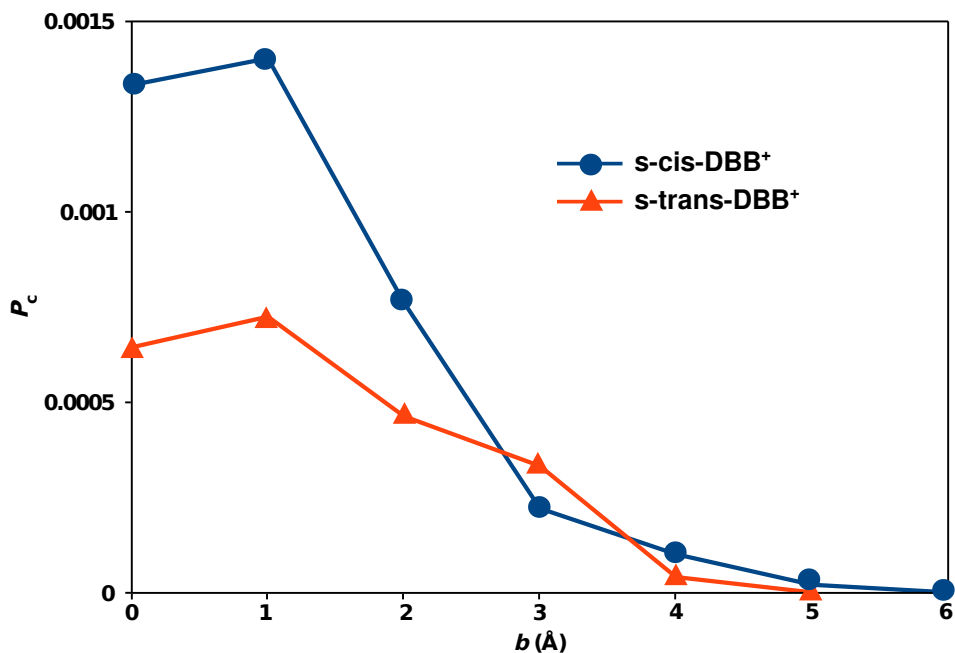


Figure 9: Opacity function for the reaction of $s\text{-cis-DBB}^+$ (blue) and $s\text{-trans-DBB}^+$ (red) with MA as a function of impact parameter b .

4 Conclusions

The cationic Diels-Alder reaction of maleic anhydride with 2,3-dibromobutadiene ions has been studied using reactive molecular dynamics. Trajectories were initiated in configurations with the two reactant molecules approaching each other mimicking a collision experiment. A competition of concerted and stepwise reaction pathways was found and both, the $s\text{-cis}$ and $s\text{-trans}$ conformers of the diene proved to be reactive. These findings are in contrast with the usual paradigm assumed for neutral Diels-Alder reactions as concerted processes in which only the $s\text{-cis}$ conformer of the diene can react. The analysis of the minimum dynamic path of the reaction indicates that both, rotations and vibrations are important to drive the system towards the transition state, whereas for the neutral reaction²⁷ only rotations were found to play an important role in promoting the reaction. This may be rationalized by the fact that the transition state of the cationic concerted reaction pathway is asymmetric, whereas the one of the neutral variant is symmetric. Because for the ionic reaction the re-

actant molecules are symmetric, deformations of the molecular structures along the reaction path are more pronounced and vibrations are more highly excited along the MDP. This analysis of the minimum dynamic path clarified the role of rotational and vibrational degrees of freedom which provides valuable information for the design of future experiments.

Another difference between the two types of reactions is that the cationic system is predicted to form van-der-Waals complexes even at the high collision energies of 50, 75, and 100 kcal/mol considered here. However, at the energies at which reactive events were recorded in the present study, the reactions were found to be direct and mostly asynchronous although some cases of synchronous trajectories were also identified. This underlines that computationally efficient energy functions are mandatory that allow running a statistically significant number of reactive trajectories such as to cover a broad range of possible scenarios. The ionic system was found to be more reactive than its neutral counterpart in line with the difference in activation energies of the two systems.

Although the accuracy of the present MS-ARMD PES is moderate compared with what is possible by using neural network⁴⁴ or kernel-based PESs,^{45–47} it needs to be stressed that running a statistically meaningful number of trajectories (here 10^6 to 10^7) for a system of the present size is currently only viable with a force field-inspired technique such as MS-ARMD. Whenever rates and quantities derived from simulations using two such different approaches have been made, they agree closely, though.^{27,43,48} Hence, although quantitative aspects of the MS-ARMD PES can be further improved, the qualitative conclusions about the reaction dynamics of the present reaction are deemed to be correct.

The present study highlights salient dynamic differences between neutral and ionic Diels-Alder reactions and represents a stepping stone towards a rigorous investigation of their dynamics in conformationally controlled gas-phase experiments.^{28,40}

Acknowledgment

Support by the Swiss National Science Foundation through grants BSCGI0_157874 (to SW), 200021_117810, 200020_188724, and the NCCR MUST (to MM), and the University of Basel is acknowledged.

References

- (1) Diels, O.; Alder, K. *Justus Liebigs Ann. Chem.* **1928**, 460, 98.
- (2) Ishihara, K.; Sakakura, A. *Comprehensive Organic Synthesis*, 2nd ed.; Elsevier: Oxford, 2014.
- (3) Houk, K. N.; González, J.; Li, Y. *Acc. Chem. Res.* **1995**, 28, 81.
- (4) Yepes, D.; Donoso-Tauda, O.; Pérez, P.; Murray, J. S.; Politzer, P.; Jaque, P. *Phys. Chem. Chem. Phys.* **2013**, 15, 7311.
- (5) de Souza, M. A. F.; Ventura, E.; do Monte, S. A.; Riveros, J. M.; Longo, R. L. *J. Comput. Chem.* **2016**, 37, 701.
- (6) Domingo, L. R. *J. Chil. Chem. Soc.* **2014**, 2615, 59.
- (7) Horn, B. A.; Herek, J. L.; Zewail, A. H. *J. Am. Chem. Soc.* **1996**, 118, 8755.
- (8) Diau, E. W.-G.; De Feyter, S.; Zewail, A. H. *Chem. Phys. Lett.* **1999**, 304, 134.
- (9) Saettel, N. J.; Wiest, O.; Singleton, D. A.; Meyer, M. P. *J. Am. Chem. Soc.* **2002**, 124, 11552.

- (10) Singleton, D. A.; Schulmeier, B. E.; Hang, C.; Thomas, A. A.; Leung, S.-W.; Merri-
gan, S. R. *Tethraedron* **2001**, *57*, 5149.
- (11) Goldstein, E.; Beno, B.; Houk, K. N. *J. Am. Chem. Soc.* **1996**, *118*, 6036.
- (12) Sakai, S. *J. Phys. Chem. A* **2000**, *104*, 922.
- (13) Domingo, L. R.; Saez, J. A. *Org. Biomol. Chem.* **2009**, *7*, 3576.
- (14) Donoghue, P. J.; Wiest, O. *Chem. Eur. J.* **2006**, *12*, 7018.
- (15) Minkin, V. I. *Pure Appl. Chem.* **1999**, *71*, 1919.
- (16) Hoffmann, R.; Woodward, R. B. *Acc. Chem. Res.* **1968**, *1*, 17.
- (17) Bellville, D. J.; Bauld, N. L. *J. Am. Chem. Soc.* **1982**, *104*, 2665.
- (18) Bauld, N. L.; Bellville, D. J.; Harirchian, B.; Lorenz, K. T.; Pabon, R. A.;
Reynolds, D. W.; Wirth, D. D.; Chiou, H.-S.; Marsh, B. K. *Acc. Chem. Res.* **1987**, *20*,
371.
- (19) Wiest, O.; Steckhan, E.; Grein, F. *J. Org. Chem.* **1992**, *57*, 4034.
- (20) Bauld, N. L.; Bellville, D. J.; Pabon, R.; Chelsky, R.; Green, G. *J. Am. Chem. Soc.*
1983, *105*, 2378.
- (21) Chockalingam, K.; Pinto, M.; Bauld, N. L. *J. Am. Chem. Soc.* **1990**, *112*, 447–448.
- (22) Eppink, A. T. J. B.; Parker, D. H. *Rev. Sci. Instrum.* **1997**, *68*, 3477.
- (23) Bouchoux, G.; Salpin, J.; Turecek, F. *Rapid Commun. Mass Spectrom.* **1994**, *8*, 325–
328.
- (24) Hofmann, M.; Schäfer III, H. F. *J. Am. Chem. Soc.* **1999**, *121*, 6719.
- (25) Bouchoux, G.; Salpin, J.-Y.; Yáñez, M. *J. Phys. Chem. A* **2004**, *108*, 9853.

- (26) Rivero, U.; Meuwly, M.; Willitsch, S. *Chem. Phys. Lett.* **2017**, *683*, 598.
- (27) Rivero, U.; Unke, O. T.; Meuwly, M.; Willitsch, S. *J. Chem. Phys.* **2019**, *151*, 104301.
- (28) Willitsch, S. *Adv. Chem. Phys.* **2017**, *162*, 307.
- (29) Brooks, B. R.; Brooks III, C. L.; Mackerell Jr., A. D.; Nilsson, L.; Petrella, R. J.; Roux, B.; Won, Y.; Archontis, G.; Bartels, C.; Boresch, S. et al. *J. Comput. Chem.* **2009**, *30*, 1545.
- (30) Nagy, T.; Reyes, J. Y.; Meuwly, M. *J. Chem. Theory Comput.* **2014**, *10*, 1366.
- (31) Atkins, P. W. *Physical Chemistry*, 5th ed.; Oxford University Press, 1994.
- (32) Verlet, L. *Phys. Rev.* **1967**, *159*, 98.
- (33) Zhao, Y.; Truhlar, D. G. *Theoretical Chemistry Accounts* **2008**, *120*, 215–241.
- (34) Hehre, W. J.; Ditchfield, R.; Pople, J. A. *J. Chem. Phys.* **1972**, *56*, 2257–2261.
- (35) Frisch, M. J.; Trucks, G. W.; Schlegel, H. B.; Scuseria, G. E.; Robb, M. A.; Cheeseman, J. R.; Scalmani, G.; Barone, V.; Mennucci, B.; Petersson, G. A. et al. Gaussian09 Revision E.01. Gaussian Inc. Wallingford CT 2009.
- (36) Zoete, V.; Cuendet, M. A.; Grosdidier, A.; Michielin, O. *J. Chem. Phys.* **2011**, *32*, 2359.
- (37) Yosa Reyes, J.; Brickel, S.; Unke, O. T.; Nagy, T.; Meuwly, M. *Phys. Chem. Chem. Phys.* **2016**, *18*, 6780–6788.
- (38) Unke, O. T.; Brickel, S.; Meuwly, M. *J. Chem. Phys.* **2019**, *150*, 074107.
- (39) Nienhaus, K.; Lutz, S.; Meuwly, M.; Nienhaus, G. U. *Chem. Eur. J.* **2013**, *19*, 3558–3562.

- (40) Chang, Y.-P.; Dlugolecki, K.; Küpper, J.; Rösch, D.; Wild, D.; Willitsch, S. *Science* **2013**, *342*, 98.
- (41) Kilaj, A.; Gao, H.; Rösch, D.; Rivero, U.; Küpper, J.; Willitsch, S. *Nature Comm.* **2018**, *9*, 2096.
- (42) Koner, D.; Barrios, L.; González-Lezana, T. s.; Panda, A. N. *J. Chem. Phys.* **2014**, *141*, 114302.
- (43) Sweeny, B. C.; Pan, H.; Kassem, A.; Sawyer, J. C.; Ard, S. G.; Shuman, N. S.; Viggiano, A. A.; Brickel, S.; Unke, O. T.; Upadhyay, M. et al. *Phys. Chem. Chem. Phys.* **2020**, *22*, 8913–8923.
- (44) Unke, O. T.; Meuwly, M. *J. Chem. Theo. Comput.* **2019**, *15*, 3678–3693.
- (45) Unke, O. T.; Meuwly, M. *J. Chem. Inf. Model.* **2017**, *57*, 1923–1931.
- (46) Chmiela, S.; Saucedo, H. E.; Mueller, K.-R.; Tkatchenko, A. *Nat. Commun.* **2018**, *9*, 3887.
- (47) Koner, D.; Meuwly, M. *arXiv preprint arXiv:2005.04667v2* **2020**,
- (48) Käser, S.; Koner, D.; Christensen, A. S.; von Lilienfeld, O. A.; Meuwly, M. *arXiv preprint arXiv:2006.16752* **2020**,

Supporting Information for

Reactive atomistic simulations of

Diels-Alder-type reactions: Conformational and

dynamic effects in the polar cycloaddition of

2,3-dibromobutadiene radical ions with maleic

anhydride

Uxia Rivero, Haydar Taylan Turan, Markus Meuwly,^{*} and Stefan Willitsch^{*}

Department of Chemistry, University of Basel, Klingelbergstrasse 80, Basel, Switzerland

E-mail: m.meuwly@unibas.ch; stefan.willitsch@unibas.ch

Abstract

1 Supplementary figures

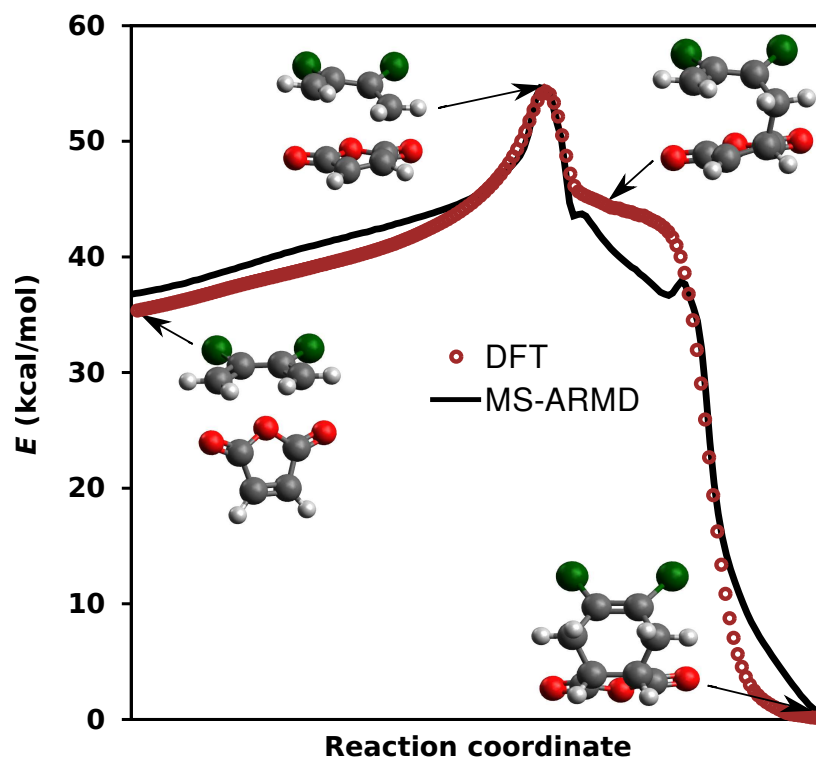


Figure S1: *Endo*-IRC at the M06-2X/6-31G* level of theory with some relevant structures along the path.

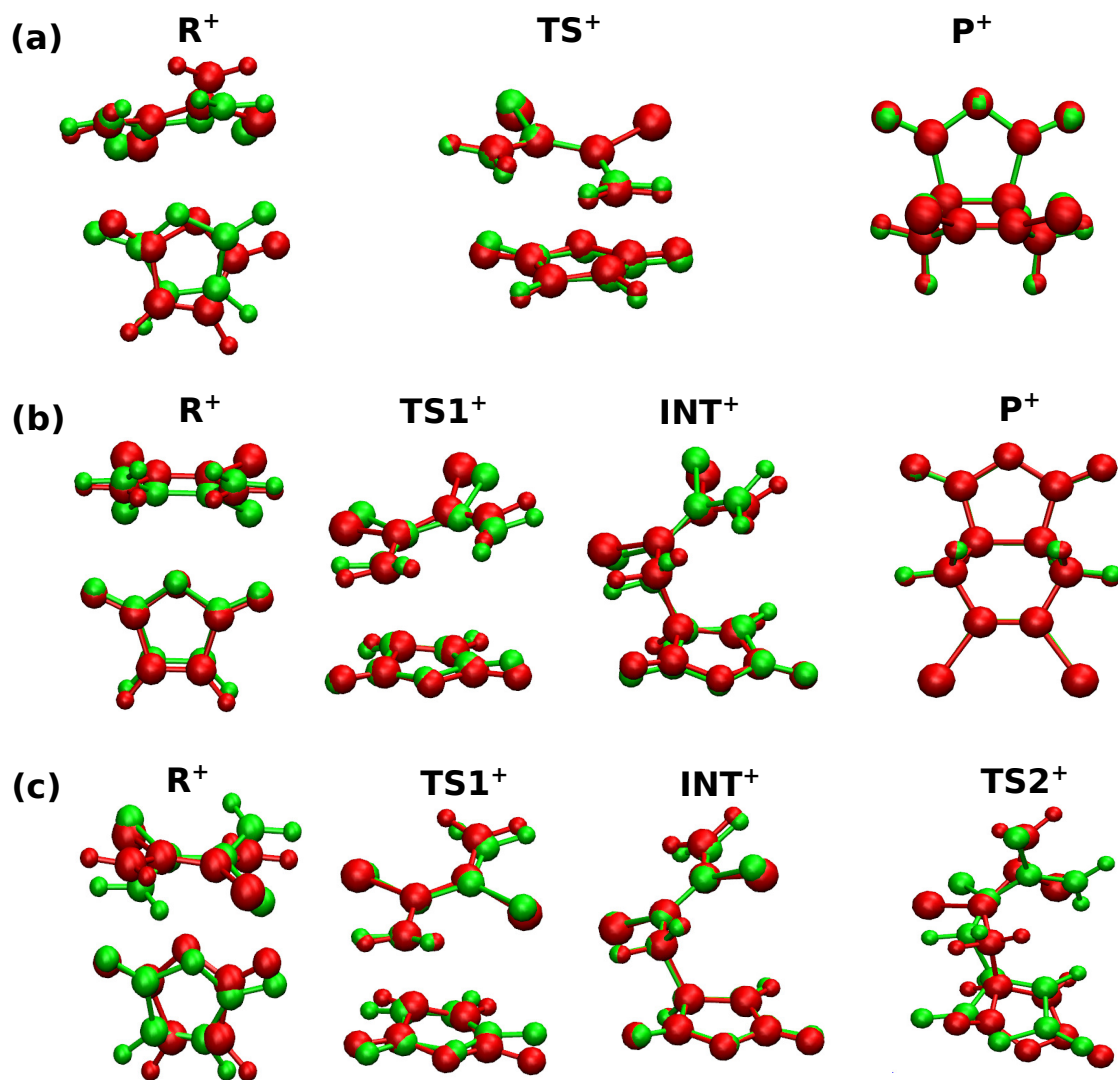


Figure S2: Comparison of optimized stationary-point structures along the (a) *endo*, (b) *exo* and (c) *trans* paths at the DFT (red) and MS-ARMD (green) levels of theory.

Table S1: RMSD between the DFT and MS-ARMD optimized stationary-point structures along the *endo*, *exo* and *trans* paths.

Molecules	RMSD (Å)
MA	0.003
cis-DBB ⁺	0.036
trans-DBB ⁺	0.083
Complexes	RMSD (Å)
TS ⁺ (<i>endo</i>)	0.325
P ⁺ (<i>endo</i>)	0.073
TS1 ⁺ (<i>exo</i>)	0.236
INT ⁺ (<i>exo</i>)	0.186
P ⁺ (<i>exo</i>)	0.074
TS1 ⁺ (<i>trans</i>)	0.270
INT ⁺ (<i>trans</i>)	0.101
TS2 ⁺ (<i>trans</i>)	0.328

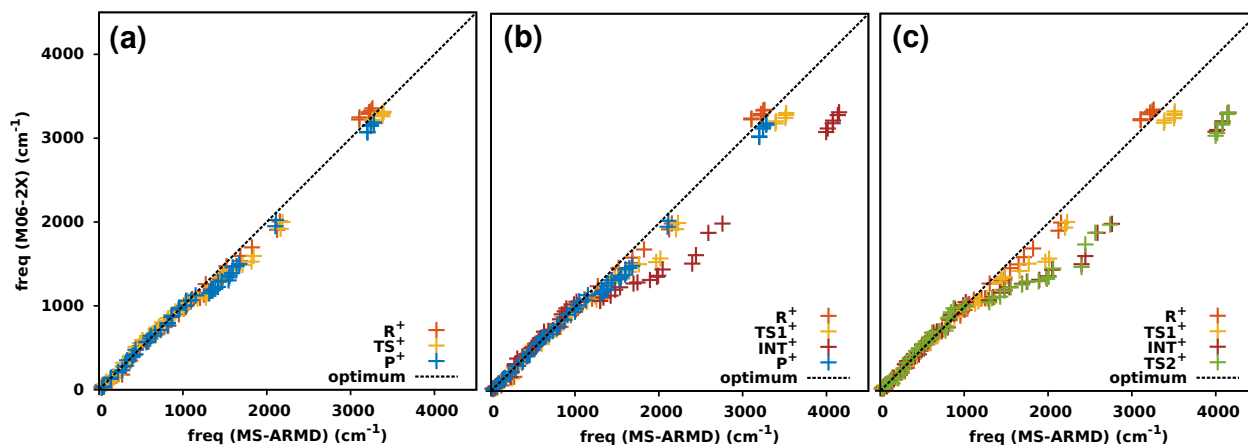


Figure S3: Comparison of harmonic frequencies at the DFT level of theory and from the MS-ARMD PES for the minimized structures along the (a) *endo*, (b) *exo* and (c) *trans* paths in Figure S2

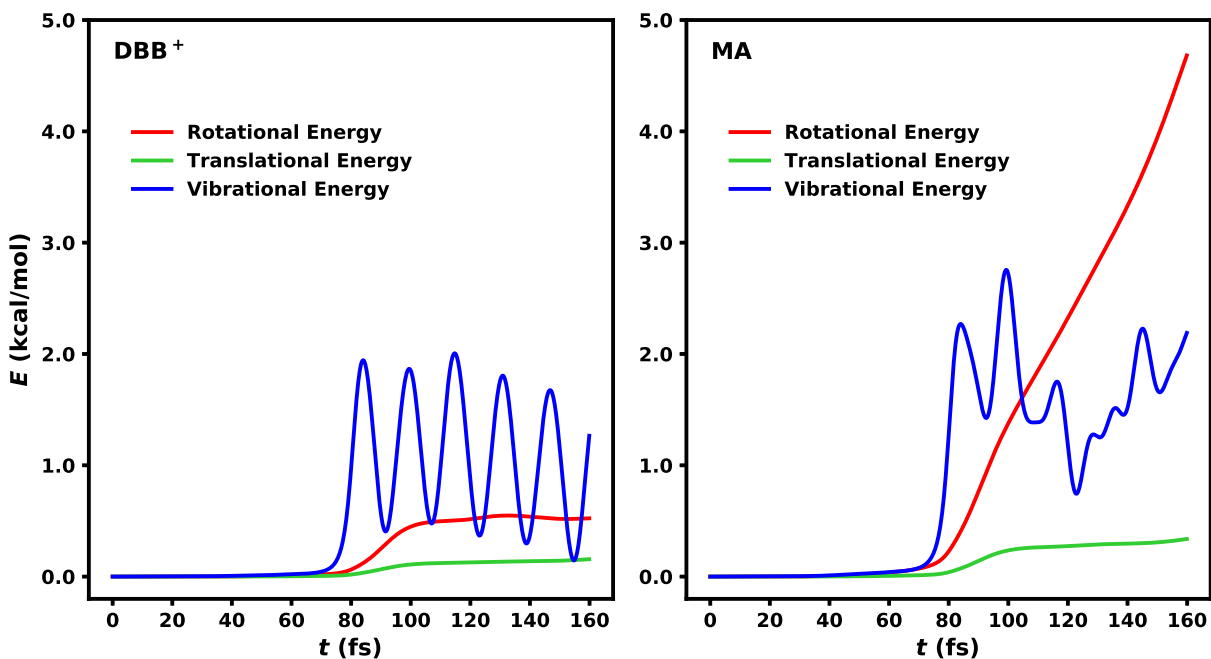


Figure S4: Decomposition of the total kinetic energy (E) along the minimum dynamic path into rotational, translational and vibrational energy. The trajectories start at TS1-exo⁺ and ends at the reactants.

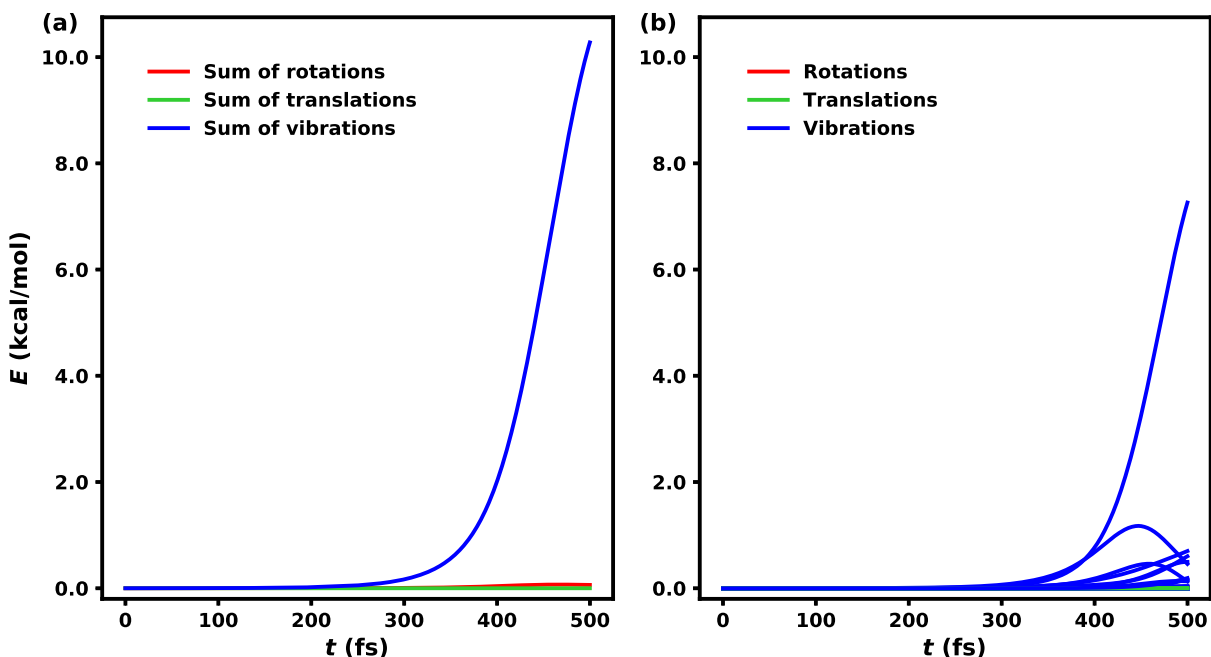


Figure S5: Projection of the total kinetic energy (E) onto the degrees of freedom of INT-tr⁺ along the minimum dynamic path for the *cis*/*trans* isomerization of the intermediate (a) summed into rotations, translations and vibrations (b) as individual traces. The trajectories start at TS2-trans⁺ and ends at INT-tr⁺. The most active vibration is the *cis*/*trans* isomerization mode.

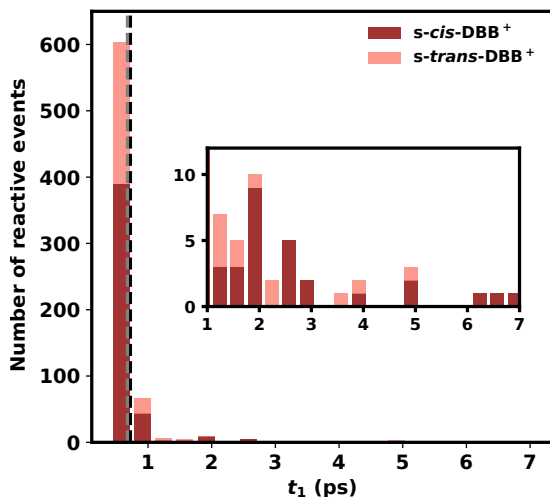


Figure S6: Stacked histogram of the time of formation of the first bond (t_1) for all reactive events. Trajectories starting with *s-cis* and *s-trans*-DBB are displayed in dark and light brown, respectively. The mean of the distributions are indicated as vertical lines in black for *s-cis*-DBB⁺ and in gray for *s-trans*-DBB⁺. The inset shows a magnification of the tail of the distribution.

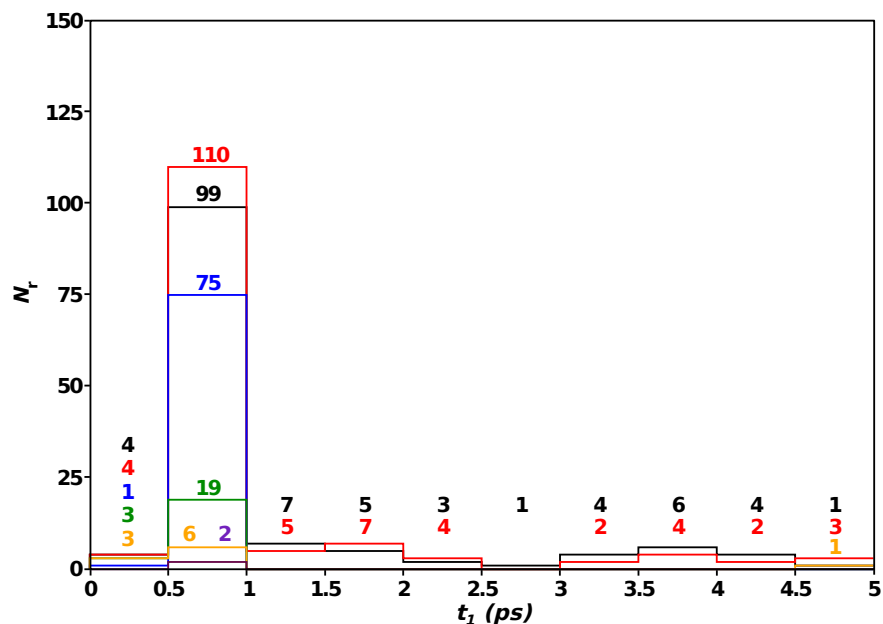


Figure S7: Stacked histogram of the formation time for the first bond (t_1) for *s-cis*-DBB⁺ with binning of 0.5 ps. Color code: $b = 0$ (black), $b \in [0, 1]$ (red), $b \in [1, 2]$ (blue), $b \in [2, 3]$ (green), $b \in [3, 4]$ (orange), $b \in [4, 5]$ (violet). The values on top of the bins represent the number of reactive trajectories within the relevant time intervals.

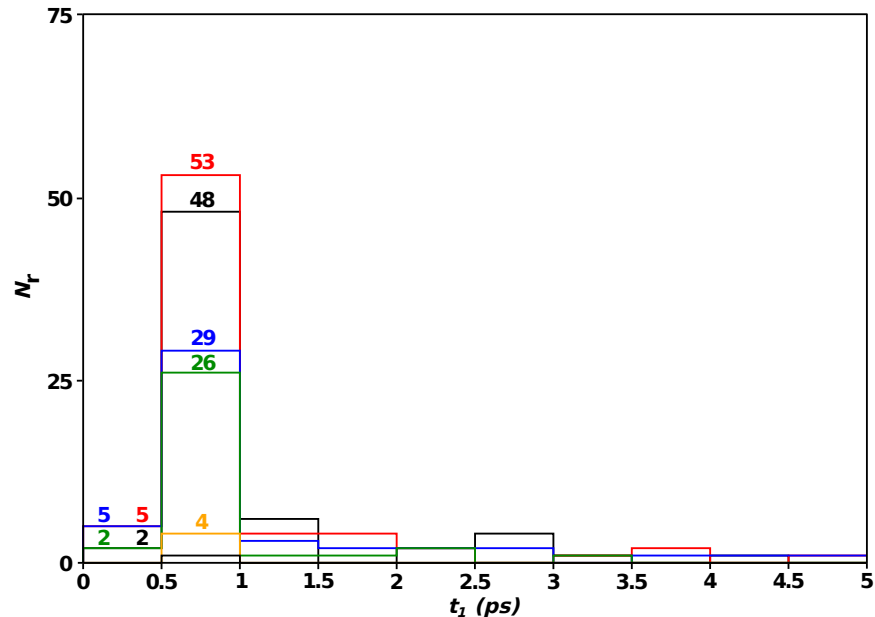


Figure S8: Stacked histogram of the formation time for the first bond (t_1) for *s-trans*-DBB⁺ with binning of 0.5 ps. Color code: $b = 0$ (black), $b \in [0, 1]$ (red), $b \in [1, 2]$ (blue), $b \in [2, 3]$ (green), $b \in [3, 4]$ (orange). The values on top of the bins represent the number of reactive trajectories within the relevant time intervals.

Parametrization of the MS-ARMD PES for the Diels-Alder reaction DBB⁺ + MA

Table S2: Harmonic bond parameters of the MS-ARMD force fields. $k/2$ is given in units of kcal/mol/Å² and r_e is in Å.

Atoms		Reactant FF		Intermediate FF		Product FF	
1 #	2 #	$k/2$	r_e	$k/2$	r_e	$k/2$	r_e
2	4	1093.65	1.19577	1398.03	1.19312	1029.89	1.19351
3	5	1093.65	1.19577	1398.03	1.19312	1029.89	1.19351
6	8	411.539	1.08513	650.507	1.08709	411.200	1.09308
7	9	411.539	1.08513	650.507	1.08709	411.200	1.09308
11	15	391.619	1.08580	650.507	1.08709	411.200	1.09308
12	17	391.619	1.08580	650.507	1.08709	411.200	1.09308
11	13	391.619	1.08580	650.507	1.08709	411.200	1.09308
10	12	391.619	1.08580	650.507	1.08709	411.200	1.09308

Table S3: Morse bond parameters for the MS-ARMD PESs. “X” indicates that this parameter is not needed. D_e is in kcal/mol, r_e in Å and β in Å⁻¹.

Atoms		Reactant FF			Intermediate FF			Product FF		
1 #	2 #	D_e	r_e	β	D_e	r_e	β	D_e	r_e	β
14	18	187.087	1.83777	1.10111	85.9534	1.81583	1.20270	91.2590	1.80871	1.89304
16	19	187.087	1.83777	1.10111	85.9534	1.81583	1.20270	91.2590	1.80871	1.89304
1	2	85.1832	1.39166	1.99423	101.912	1.34206	1.87376	474.144	1.37373	1.00021
1	3	85.1832	1.39166	1.99423	101.912	1.34206	1.87376	474.144	1.37373	1.00021
2	6	164.953	1.50368	1.40025	63.8103	1.55906	1.18897	189.327	1.52650	1.38405
3	7	164.953	1.50368	1.40025	63.8103	1.55906	1.18897	189.327	1.52650	1.38405
14	16	564.329	1.40983	0.896631	327.948	1.41861	1.44211	310.137	1.42532	1.12287
11	14	189.781	1.36281	1.63991	76.1220	1.32884	1.01309	236.306	1.49451	1.24374
12	16	189.781	1.36281	1.63991	76.1220	1.32884	1.01309	236.306	1.49451	1.24374
6	7	194.950	1.33603	1.99291	154.586	1.50359	1.94850	58.3539	1.47745	1.99994
7	12	X	X	X	116.127	1.51263	1.01790	58.3539	1.47745	1.99994
6	11	X	X	X	X	X	X	58.3539	1.47745	1.99994

Table S4: Angle parameters for the MS-ARMD PESs. “X” indicates that this parameter is not needed. $k/2$ is in kcal/mol/radian², θ_e in degree

Atoms			Reactant FF		Intermediate FF		Product FF	
1 #	2 #	3 #	$k/2$	θ_e	$k/2$	θ_e	$k/2$	θ_e
2	1	3	64.5319	105.978	135.149	97.7709	109.386	111.098
1	2	4	99.6847	128.737	165.070	130.560	114.817	135.968
1	2	6	135.436	109.951	277.466	107.951	134.612	120.559
4	2	6	77.1982	137.451	78.2342	143.084	71.8608	148.445
1	3	5	99.6847	128.737	165.070	130.560	114.817	135.968
1	3	7	135.436	109.951	277.466	107.951	134.612	120.559
5	3	7	77.1982	137.451	78.2342	143.084	71.8608	148.445
2	6	7	95.5494	108.805	134.514	110.650	89.4152	108.264
2	6	8	38.5239	124.711	67.2617	121.288	61.0991	109.775
2	6	11	X	X	X	X	89.4152	108.264
7	6	8	20.1303	129.751	64.9256	125.690	54.6427	108.583
7	6	11	X	X	X	X	82.9790	98.3030
8	6	11	X	X	X	X	54.6427	108.583
3	7	6	95.5494	108.805	134.514	110.650	89.4152	108.264
3	7	9	38.5239	124.711	67.2617	121.288	61.0991	109.775
3	7	12	X	X	134.514	110.650	89.4152	108.264
6	7	9	20.1303	129.751	64.9256	125.690	54.6427	108.583
6	7	12	X	X	35.4515	133.262	82.9790	98.3030
9	7	12	X	X	64.9256	125.690	54.6427	108.583
6	11	13	X	X	X	X	54.6427	108.583
6	11	14	X	X	X	X	65.2956	104.164
6	11	15	X	X	X	X	54.6427	108.583
13	11	14	44.8358	132.443	123.161	121.235	58.4988	108.370
13	11	15	30.0806	138.270	106.624	119.564	44.9477	107.173
14	11	15	44.8358	132.443	123.161	121.235	58.4988	108.370
7	12	10	X	X	64.9256	125.690	54.6427	108.583
7	12	16	X	X	46.2212	134.655	65.2956	104.164
7	12	17	X	X	64.9256	125.690	54.6427	108.583
10	12	16	44.8358	132.443	123.161	121.235	58.4988	108.370
10	12	17	30.0806	138.270	106.624	119.564	44.9477	107.173
16	12	17	44.8358	132.443	123.161	121.235	58.4988	108.370
11	14	16	112.001	124.423	57.8435	132.115	92.0564	132.027
11	14	18	43.8118	136.630	46.9468	138.569	51.8620	130.256
16	14	18	50.3729	127.032	22.9482	148.260	81.7961	128.923
12	16	14	112.001	124.423	57.8435	132.115	92.0564	132.027
12	16	19	43.8118	136.630	46.9468	138.569	51.8620	130.256
14	16	19	50.3729	127.032	22.9482	148.260	81.7961	128.923

Table S5: Dihedral parameters of the MS-ARMD PESs. “X” indicates that this parameter is not needed. k is in kcal/mol and ϕ in degree.

Atoms					Reactant FF	Intermediate FF	Product FF	
1 #	2 #	3 #	4 #	N	k	k	k	ϕ
1	2	6	7	1	X	-4.14146	-0.523798	0.00
1	2	6	7	2	4.79788	8.55575	1.72536	180.00
1	2	6	7	3	X	-1.81563	0.267926	0.00
1	2	6	8	2	0.249864	2.35984	2.15011	180.00
1	2	6	8	3	X	0.221796	1.66411	0.00
1	2	6	11	1	X	X	-0.523798	0.00
1	2	6	11	2	X	X	1.72536	180.00
1	2	6	11	3	X	X	0.267926	0.00
1	3	7	6	1	X	-4.14146	-0.523798	0.00
1	3	7	6	2	4.79788	8.55575	1.72536	180.00
1	3	7	6	3	X	-1.81563	0.267926	0.00
1	3	7	9	2	0.249864	2.35984	2.15011	180.00
1	3	7	9	3	X	0.221796	1.66411	0.00
1	3	7	12	1	X	-4.14146	-0.523798	0.00
1	3	7	12	2	X	8.55575	1.72536	180.00
1	3	7	12	3	X	-1.81563	0.267926	0.00
2	1	3	5	1	0.701169	-5.58519	-0.126467	0.00
2	1	3	5	2	6.21522	-9.49140	-5.49755	180.00
2	1	3	5	3	0.298850	12.7562	3.34467	0.00
2	1	3	7	2	7.17573	-1.12647	4.91803	180.00
2	6	7	3	1	X	-3.95005	-1.29628	0.00
2	6	7	3	2	8.19928	-1.12703	X	X
2	6	7	3	3	X	0.390811	0.330764	0.00

Atoms					Reactant FF	Intermediate FF	Product FF	
1 #	2 #	3 #	4 #	N	k	k	k	ϕ
2	6	7	9	1	X	1.45039	0.336052	0.00
2	6	7	9	2	6.34212	-0.211970	-2.95419	180.00
2	6	7	12	1	X	-5.40684	-3.89326	0.00
2	6	7	12	2	X	0.454822	-2.88140	180.00
2	6	7	12	3	X	-0.0439145	-0.444273	0.00
2	6	11	13	1	X	X	0.336052	0.00
2	6	11	13	2	X	X	-2.95419	180.00
2	6	11	14	3	X	X	0.035506	0.00
2	6	11	15	1	X	X	0.336052	0.00
2	6	11	15	2	X	X	-2.95419	180.00
3	1	2	4	1	0.701169	-5.58519	-0.126467	0.00
3	1	2	4	2	6.21522	-9.49140	-5.49755	180.00
3	1	2	4	3	0.298850	12.7562	3.34467	0.00
3	1	2	6	2	7.17573	12.7562	3.34467	180.00
3	7	6	8	1	X	1.45039	0.336052	0.00
3	7	6	8	2	6.34212	-0.211970	-2.95419	180.00
3	7	6	11	1	X	X	-3.89326	0.00
3	7	6	11	2	X	X	-2.88140	180.00
3	7	6	11	3	X	X	-0.444273	0.00
3	7	12	10	1	X	1.45039	0.336052	0.00
3	7	12	10	2	X	-0.211970	-2.95419	180.00
3	7	12	16	3	X	1.51659	0.035506	0.00
3	7	12	17	1	X	1.45039	0.336052	0.00
3	7	12	17	2	X	-0.211970	-2.95419	180.00
4	2	6	7	1	X	-9.15296	-2.89358	0.00

Atoms					Reactant FF	Intermediate FF	Product FF	
1 #	2 #	3 #	4 #	N	k	k	k	ϕ
4	2	6	7	2	-0.999624	-1.25200	1.75806	180.00
4	2	6	8	1	X	-10.0609	-2.16831	0.00
4	2	6	8	2	2.45356	-2.58269	1.09179	180.00
4	2	6	8	3	X	-1.46073	0.192876	0.00
4	2	6	11	1	X	X	-2.89358	0.00
4	2	6	11	2	X	X	1.75806	180.00
4	2	6	11	3	X	X	0.230563	0.00
5	3	7	6	1	X	-9.15296	-2.89358	0.00
5	3	7	6	2	-0.999624	-1.25200	1.75806	180.00
5	3	7	6	3	X	-0.997410	0.230563	0.00
5	3	7	9	1	X	-10.0609	-2.16831	0.00
5	3	7	9	2	2.45356	-2.58269	1.09179	180.00
5	3	7	9	3	X	-1.46073	0.192876	0.00
5	3	7	12	1	X	-9.15296	-2.89358	0.00
5	3	7	12	2	X	-1.25200	1.75806	180.00
5	3	7	12	3	X	-0.997410	0.230563	0.00
6	7	12	10	1	X	-6.25427	-1.53021	0.00
6	7	12	10	2	X	-0.819813	-0.713956	180.00
6	7	12	10	3	X	-1.40487	-0.0941236	0.00
6	7	12	16	1	X	0.0503902	-1.74289	0.00
6	7	12	16	2	X	1.43493	-2.69254	180.00
6	7	12	16	3	X	5.08310	-2.56013	0.00
6	7	12	17	1	X	-6.25427	-1.53021	0.00
6	7	12	17	2	X	-0.819813	-0.713956	180.00
6	7	12	17	3	X	-1.40487	-0.0941236	0.00

Atoms					Reactant FF	Intermediate FF	Product FF	
1 #	2 #	3 #	4 #	N	k	k	k	ϕ
6	11	14	16	1	X	X	-2.46899	0.00
6	11	14	16	2	X	X	0.0047732	180.00
6	11	14	16	3	X	X	-0.713956	0.00
6	11	14	18	1	X	X	0.000	0.00
7	6	11	13	1	X	X	-1.53021	0.00
7	6	11	13	2	X	X	-0.713956	180.00
7	6	11	13	3	X	X	-0.094123	0.00
7	6	11	14	1	X	X	-1.74289	0.00
7	6	11	14	2	X	X	-2.69254	180.00
7	6	11	14	3	X	X	-2.56013	0.00
7	6	11	15	1	X	X	-1.53021	0.00
7	6	11	15	2	X	X	-0.713956	180.00
7	6	11	15	3	X	X	-0.0941236	0.00
7	12	16	14	1	X	1.56618	-1.74289	0.00
7	12	16	14	2	X	-2.45376	0.0047732	180.00
7	12	16	14	3	X	-0.819813	-0.713956	0.00
7	12	16	19	1	X	0.000	0.000	0.00
8	6	7	9	1	X	-3.43664	-0.0510087	0.00
8	6	7	9	2	2.34735	1.24857	-2.28477	180.00
8	6	7	9	3	X	1.78467	0.0546769	0.00
8	6	7	12	1	X	-6.25427	-1.53021	0.00
8	6	7	12	2	X	-0.819813	-0.713956	180.00
8	6	7	12	3	X	-1.40487	-0.094123	0.00
8	6	11	13	1	X	X	-0.051008	0.00
8	6	11	13	2	X	X	-2.28477	180.00

Atoms					Reactant FF	Intermediate FF	Product FF	
1 #	2 #	3 #	4 #	N	k	k	k	ϕ
8	6	11	13	3	X	X	0.0546769	0.00
8	6	11	14	1	X	X	0.861788	0.00
8	6	11	14	2	X	X	0.995909	180.00
8	6	11	14	3	X	X	-1.07686	0.00
8	6	11	15	1	X	X	-0.051008	0.00
8	6	11	15	2	X	X	-2.28477	180.00
8	6	11	15	3	X	X	0.0546769	0.00
9	7	6	11	1	X	X	-1.53021	0.00
9	7	6	11	2	X	X	-0.713956	180.00
9	7	6	11	3	X	X	-0.0941236	0.00
9	7	12	10	1	X	-3.43664	-0.0510087	0.00
9	7	12	10	2	X	1.24857	-2.28477	180.00
9	7	12	10	3	X	1.78467	0.054676	0.00
9	7	12	16	1	X	-1.19475	0.861788	0.00
9	7	12	16	2	X	3.74789	0.995909	180.00
9	7	12	16	3	X	-1.42060	-1.07686	0.00
9	7	12	17	1	X	-3.43664	-0.0510087	0.00
9	7	12	17	2	X	1.24857	-2.28477	180.00
9	7	12	17	3	X	1.78467	0.0546769	0.00
10	12	16	14	1	X	-4.27768	-3.29003	0.00
10	12	16	14	2	3.21391	3.74789	0.995909	180.00
10	12	16	14	3	X	0.960659	-0.693868	0.00
10	12	16	19	1	X	2.13188	0.000	0.00
10	12	16	19	2	2.53826	-3.11705	X	X
11	6	7	12	1	X	X	-0.601273	0.00

Atoms					Reactant FF	Intermediate FF	Product FF	
1 #	2 #	3 #	4 #	N	k	k	k	ϕ
11	6	7	12	2	X	X	5.54093	180.00
11	6	7	12	3	X	X	-1.18306	0.00
11	14	16	12	1	-0.818383	-2.27656	-5.28649	0.00
11	14	16	12	2	1.645260	3.43143	2.36666	180.00
11	14	16	12	3	-1.23972	-2.35012	X	X
11	14	16	19	2	3.07771	0.554677	2.36666	180.00
12	16	14	18	2	3.07771	0.554677	2.36666	180.00
13	11	14	16	1	X	-4.27768	-3.29003	0.00
13	11	14	16	2	2.42160	3.74789	0.995909	180.00
13	11	14	16	3	X	0.960659	-0.693868	0.00
13	11	14	18	1	X	0.000	0.000	0.00
13	11	14	18	2	2.53826	-3.11705	X	X
14	16	12	17	1	X	-4.27768	-3.29003	0.00
14	16	12	17	2	3.21391	3.74789	0.995909	180.00
14	16	12	17	3	X	0.960659	-0.693868	0.00
15	11	14	16	1	X	-4.27768	-3.29003	0.00
15	11	14	16	2	2.42160	3.74789	0.995909	180.00
15	11	14	16	3	X	0.960659	-0.693868	0.00
15	11	14	18	1	X	0.000	0.000	0.00
15	11	14	18	2	2.53826	-3.11705	X	X
17	12	16	19	1	X	0.000	0.000	0.00
17	12	16	19	2	2.53826	-3.11705	X	X
18	14	16	19	2	3.13276	3.43143	2.36666	180.00

Table S6: Non-bonded parameters of the MS-ARMD reactant PES. “X” indicates that this parameter is not needed.

Atom #	q_i [e]	$\epsilon_{i,1}$ [kcal/mol]	$R_{min,1}/2[\text{\AA}]$	$\epsilon_{i,2}$ [kcal/mol]	$R_{min,2}/2[\text{\AA}]$
1	-0.300000	0.203207E-04	2.80541	X	X
2	0.705600	0.667655	0.102478	X	X
3	0.705600	0.667655	0.102478	X	X
4	-0.570000	0.411920E-08	4.77007	0.120	1.40
5	-0.570000	0.411920E-08	4.77007	0.120	1.40
6	-0.135600	0.242868E-01	2.13203	X	X
7	-0.135600	0.242868E-01	2.13203	X	X
8	0.150000	0.218559	0.917005	X	X
9	0.150000	0.218559	0.917005	X	X
10	0.152910	0.218559	0.917005	X	X
11	0.221270	0.242868E-01	2.13203	X	X
12	0.221270	0.242868E-01	2.13203	X	X
13	0.152910	0.218559	0.917005	X	X
14	-0.151030	0.242868E-01	2.13203	X	X
15	0.152910	0.218559	0.917005	X	X
16	-0.151030	0.242868E-01	2.13203	X	X
17	0.152910	0.218559	0.917005	X	X
18	0.139550	0.648973E-01	2.32950	X	X
19	0.139550	0.648973E-01	2.32950	X	X
Atom 1 #	Atom 2#	ϵ_i [kcal/mol]	$R_{min}/2[\text{\AA}]$	n	m
18	4	2.76499	3.30525	15.5903	16.2486
18	5	2.76499	3.30525	15.5903	16.2486
19	4	2.76499	3.30525	15.5903	16.2486
19	5	2.76499	3.30525	15.5903	16.2486
11	6	6.23430	2.25895	3.34975	5.24917
12	7	6.23430	2.25895	3.34975	5.24917
11	7	6.23430	2.25895	3.34975	5.24917
12	6	6.23430	2.25895	3.34975	5.24917

Table S7: Non-bonded parameters of the MS-ARMD intermediate PES. “X” indicates that this parameter is not needed.

Atom #	q_i [e]	$\epsilon_{i,1}$ [kcal/mol]	$R_{min,1}/2[\text{\AA}]$	$\epsilon_{i,2}$ [kcal/mol]	$R_{min,2}/2[\text{\AA}]$
1	-0.287170	0.152100	1.770000	X	X
2	0.545440	0.110000	2.000000	X	X
3	0.545440	0.110000	2.000000	X	X
4	-0.392740	0.120000	1.700000	0.120	1.40
5	-0.392740	0.120000	1.700000	0.120	1.40
6	-0.408260E-01	0.055000	2.175000	0.010	1.90
7	-0.408260E-01	0.055000	2.175000	0.010	1.90
8	0.104730	0.022000	1.320000	X	X
9	0.104730	0.022000	1.320000	X	X
10	0.195520	0.022000	1.320000	X	X
11	-0.803190E-01	0.055000	2.175000	0.010	1.90
12	-0.803190E-01	0.055000	2.175000	0.010	1.90
13	0.195520	0.022000	1.320000	X	X
14	-0.914950E-01	0.068000	2.090000	X	X
15	0.883190E-01	0.022000	1.320000	X	X
16	-0.914950E-01	0.068000	2.090000	X	X
17	0.883190E-01	0.022000	1.320000	X	X
18	0.321120	4.35177	1.69104	X	X
19	0.321120	4.35177	1.69104	X	X
Atom 1 #	Atom 2#	ϵ_i [kcal/mol]	$R_{min}/2[\text{\AA}]$	n	m
18	4	5.24581	3.55543	3.04411	4.51621
18	5	5.24581	3.55543	3.04411	4.51621
19	4	5.24581	3.55543	3.04411	4.51621
19	5	5.24581	3.55543	3.04411	4.51621
11	6	4.20015	1.90058	3.53818	5.54809
11	7	4.20015	1.90058	3.53818	5.54809

Table S8: Non-bonded parameters of the MS-ARMD product PES. “X” indicates that this parameter is not needed.

Atom #	q_i [e]	$\epsilon_{i,1}$ [kcal/mol]	$R_{min,1}/2[\text{\AA}]$	$\epsilon_{i,2}$ [kcal/mol]	$R_{min,2}/2[\text{\AA}]$
1	-0.285000	0.152100	1.770000	X	X
2	0.568000	0.110000	2.000000	X	X
3	0.568000	0.110000	2.000000	X	X
4	-0.414000	0.120000	1.700000	0.120	1.40
5	-0.414000	0.120000	1.700000	0.120	1.40
6	-0.034000	0.055000	2.175000	0.010	1.90
7	-0.034000	0.055000	2.175000	0.010	1.90
8	0.11240	0.022000	1.320000	X	X
9	0.11240	0.022000	1.320000	X	X
10	0.19260	0.022000	1.320000	X	X
11	-0.055200	0.055000	2.175000	0.010	1.90
12	-0.055200	0.055000	2.175000	0.010	1.90
13	0.19260	0.022000	1.320000	X	X
14	-0.126000	0.068000	2.090000	X	X
15	0.08290	0.022000	1.320000	X	X
16	-0.126000	0.068000	2.090000	X	X
17	0.08290	0.022000	1.320000	X	X
18	0.317000	3.99998	1.67206	X	X
19	0.317000	3.99998	1.67206	X	X

The barrier region connecting the reactant and intermediate force fields and the intermediate and product force fields is described by two GAPOs $\Delta V_{\text{GAPO},k}^{ij}(x) = \exp\left(-\frac{(\Delta V_{ij}(x) - V_{ij,k}^0)^2}{2\sigma_{ij,k}^2}\right) \times \sum_{l=0}^{m_{ij,k}} a_{ij,kl}(\Delta V_{ij}(x) - V_{ij,k}^0)^l$ with the parameters summarized in Table S9.

Table S9: GAPO parameters: i labels the reactant (R^+) or the intermediate (INT^+) and j labels the intermediate or the product (P^+), $V_{ij,k}^0$ is the center of the Gaussian function (in kcal/mol), and $\sigma_{ij,k}$ the width of the Gaussian (in kcal/mol). a_{ij} is the polynomial coefficient in $(\text{kcal/mol})^{1-j}$, $j = 0, 3$.

i	j	k	$V_{ij,k}^0$	$\sigma_{ij,k}$	$a_{ij,k0}$	$a_{ij,k1}$	$a_{ij,k2}$	$a_{ij,k3}$
R^+	INT^+	3	2.2385E+01	2.5180E+01	-1.5000E+01	3.9005E-01	-1.0249E-02	1.1676E-04
INT^+	P^+	2	-2.8049E+01	3.5355E+01	-1.2000E+01	-4.8562E-01	-5.6894E-03	